2008

Chemical mechanical planarization: Study of conditioner abrasives and synthesis of nano-zirconia for potential slurry applications

Chhavi Manocha
University of South Florida

Chemical Mechanical Planarization: Study of Conditioner Abrasives and Synthesis of Nano-Zirconia for Potential Slurry Applications

by

Chhavi Manocha

A thesis submitted in partial fulfillment
of the requirements for the degree of
Master of Chemical Engineering
Department of Chemical and Biomedical Engineering
College of Engineering
University of South Florida

Co-Major Professor: Vinay K. Gupta, Ph.D.
Co-Major Professor: Ashok Kumar, Ph.D.
Andrew M. Hoff, Ph.D.
John T. Wolan, Ph.D.

Date of Approval:
October 31, 2008

Keywords: chemical mechanical polishing, conditioning, pad wear, contact area, plasma synthesis

Dedication

I dedicate my thesis to my parents, Dr. L. M. Manocha and Dr. S. Manocha. Their constant support, encouragement and guidance always made it possible for me to sail through the toughest times and believe in myself**.**

Acknowledgements

I take this opportunity to thank my advisors, Dr. Vinay K. Gupta and Dr. Ashok Kumar, for their help and guidance throughout my research work. I would also like to thank Dr. Anandan for his constant support and encouragement. Some of the work presented here was done during my summer internship at 3M. I would like to thank Rajesh Katare for giving me an opportunity to work on the Plasma synthesis, Dr. Gundu Sabde and Gary Palmgren for the work done on optical microscopy. I'd like to express my gratitude towards Dr. Raghu Mudhivarthi, Dr. Makoto Hirai and Cecil Coutinho for introducing me to the subject and helping me with my experiments**.**

Table of Contents

List of Tables

List of Figures

Chemical Mechanical Planarization: Study of Conditioner Abrasives and Synthesis of Nano-Zirconia for Potential Slurry Applications

Chhavi Manocha

ABSTRACT

Chemical Mechanical Planarization (CMP) has emerged as the central technology for polishing wafers in the semiconductor manufacturing industry to make integrated multi-level devices. As the name suggests, both chemical and mechanical processes work simultaneously to achieve local and global planarization. In spite of extensive work done to understand the various components and parameters affecting the performance of this process, many aspects of CMP remain poorly understood. Among these aspects of CMP is the role of abrasives in the processes of conditioning and polishing. These abrasives are present in the chemical slurry between the wafer and the pad for polishing and play an important role during the conditioning to regenerate the clogged polishing pads.

This thesis has focused on the study of abrasives, both in conditioning and polishing. The first part of the thesis concentrates on the effect of abrasive size for conditioning purposes. Diamond is being widely used as an abrasive for conditioning the polishing pad. Five different sizes of diamonds ranging from 0.25μm to 100μm were selected to condition the commercially available IC 1000 polishing pad. Scanning Electron Microscopy (SEM) and Atomic Force Microscopy (AFM) analysis were carried

out on the pad to study the effect of the abrasive size on the pad morphology. In-situ 'coefficient of friction' was also monitored on the CETR bench top Tester. The final impact was seen in the form of surface defects on the polished copper wafers. As pad morphologies resulting from different conditioning affect contact areas, the second part of the thesis focuses on developing a simple method to quantify the area of contact between the wafer and pad using optical microscopy. Optical images that were obtained were analyzed for the change in contact area with the change in operating conditions. Finally, the third part of the thesis details the synthesis and characterization of nano-zirconia for potential slurry applications. Nano-zirconia was synthesized using the plasma route and then characterized using different analytical techniques like TEM and XRD. These nanoparticles were then used to make abrasive slurry for oxide CMP and the polished wafers were analyzed for surface defects.

Chapter 1

Introduction and Background

To enable superior IC performance, it is critical to reduce device dimensions. As the devices become smaller several challenges arise in their design and fabrication. After fabrication of the devices on the silicon substrate, metallic interconnects are used to interface these devices with each other and to the outside world. At the silicon level, the devices are interconnected using metallization, which is referred to as the first level of metallization. The connections between the device network and the outside world are referred to as the second level of metallization. In order to successfully build a multilevel metallization structure, the surfaces of each previous metal layer has to be perfectly flat. In the absence of planarity, the irregular surfaces and uneven thicknesses lead to an inefficient pattern transfer (Figure 1.1). A planarized surface promotes homogeneous thickness of metal layers and results in lowering the level defects and the electro migration effects. Thus, planarization plays an important role in the semiconductor industry.

1.1. Planarization techniques

Wafer planarization may be classified into three categories of planarity. These are summarized below (*1, 2*):

Surface Smoothing: Feature corners are smoothed and high aspect ratio holes are filled as in Figure 1.2.

1. Local planarity: Surfaces are flat locally, but the surface height may vary across the die as in Figure 1.3.
2. Global planarity: The surface is flat across the entire stepper field as in Figure 1.4.

The requirement for surface smoothing and local planarity comes from metal step coverage, which is defined by the ratio of thinnest point in metal film to the thickest point in metal film (*3*). The requirement for global planarity increases when the circuit dimensions reach sub-0.5µ. Several techniques exist to achieve local and global planarization. Different planarization processes are seen to achieve different degrees of planarity. Some of these techniques are discussed below.

Doped Gas Reflow: One of the first planarization techniques used in the IC industry involved the synthesis of low pressure chemical vapor deposited (LPCVD) boron and phosphorous doped silicon oxide (*4, 5*). This was used for the planarization of the first layer of dielectric. Better smoothing of step corners could be achieved by doping SiO2 with boron and phosphorous.

Spin Etch Planarization: Spin Etch Planarization is based on the principles of controlled chemical etching of metals (*6*). In this process, the wafer is suspended horizontally on a nitrogen cushion above a rotating chuck. Locking pins are used on the edge of the wafer to locate the substrate laterally. Wet etch chemistries are dispensed into the wafer, as it is being rotated by the chuck. Using an appropriate etching solution, the planar surface is achieved while the wafer is being rotated and excess Cu is removed.

Spin on Deposition**:** In this process, the base catalyst and necessary organic additives are mixed at room temperature to prepare the precursor solution for the material to be deposited. Pretreating of the wafer surface is conducted in order to promote sol spreading. The sol is dripped on the wafer while it is spinning. The wafer is then rinsed, spun dried, baked, and then cured. It results in local planarization (*7*).

1.2. Chemical Mechanical Planarization

As discussed earlier, the process of smoothening and planing a surface is referred to as planarization. When the smoothening and planning of surfaces is aided by chemical and mechanical forces, it is referred to as Chemical Mechanical Planarization (CMP). Chemical Mechanical Planarization was introduced by IBM to facilitate planarization of inter-level dielectrics (*8*). In addition, CMP is also used to polish multiple materials in a Damascene process. Chemical Mechanical Planarization or CMP is the method of choice for achieving local and global planarity in the wafers. As the name suggests, CMP is a combination of chemical and mechanical processes working at the same time to achieve planarization. Further, the ongoing chemical reaction is seen to enhance the mechanical removal rate. The key to achieving planarity is maintaining high removal rate at high surface features and low removal rates at low surface features (*9*).

1.2.1. Working of the CMP process

Figure 1.5 shows the schematic of the CMP process. The CMP polisher consists of a bottom rotating platen on which a polishing pad is fixed. The top platen holds the wafer to be polished, face down on the pad. During the polishing run, the wafer comes in contact with the pad surface with a set downforce. Both the platens rotate during the run.

Polishing slurry consisting of abrasive particles and other necessary chemical constituents are fed to the pad surface to carry out the polishing where the pad comes in contact with the wafer being polished. The abrasive slurry has several functions. It provides the necessary chemical input for the planarization process, acts as a lubricant to maintain the temperature caused due to the friction and also transports the particles across the polishing surface. The pad used for polishing is seen to glaze under the effect of polishing. To get higher removal rates, the pad needs to be regenerated. This is done by conditioning, which is the second stage of the CMP process. The rotating polishing pad is abraded using a conditioner which is an abrasive disk that opens up the clogged pores of the pad.

The polishing mechanism can be explained on the basis of the contacts occurring in the system. The chemicals in the slurry, on contact with the wafer, soften the wafer surface, while the abrasives in the slurry remove this layer. In the absence of the mechanical fraction, the chemical effect is limited.

1.2.2. CMP mechanism

The polishing takes place at points where the wafer surface comes in contact with the surface of the pad, which in turn holds the slurry particles. This mechanism is best described by the Preston's law, which states that the material removal rate is directly proportional to the applied pressure and relative velocity of the particles(*10*).
The mathematical expression for the law is given by the equation shown below.

$$RR = K_P.P.V$$

RR = Removal rate; P = Applied pressure;

V = Velocity; K_P = Preston's constant;

Preston's equation is an empirical law. It shows a linear dependence of removal rate on pressure and relative velocity. Preston's constant accounts for the other chemical and physical parameters involved in polishing. The Polishing pad surface gets more compressed by the raised wafer surfaces, which results in higher pressure giving higher removal rates.

1.2.3. Input and output variables in CMP

The CMP process is quite complicated and involves a large number of input and output variables. The different output variables include polish rate, planarization rate, surface quality, surface damage, and feature size dependence.

1. Polish Rate: The polish rate is defined as the ratio of the thickness of the film removed to the polish time. Its units are either mm/min or μm/min. Higher polish rates imply shorter polish times and are hence, desirable. However, controlling the process is difficult when the polish rates go higher.
2. Planarization Rate: Planarization rate is defined in terms of the time taken to reduce the topography of a surface to the desired level.
3. Surface Quality: The expected yield and reliability of the interconnections are dependent on the surface quality. The surface quality can be improved and roughness minimized by properly balancing the chemical and mechanical components of the CMP process.
4. Surface Damage: Damage may occur to metal films, which directly affects the yield and reliability of the interconnections. Structural damage may include scratches, delamination of the film interfaces, introduction of impurities in the film, etc.

In case of input variables, four broad categories can be used: Wafer, slurry, polishing pad and operating conditions.

1. Wafer: The wafer to be polished determines the other associated input variables for polishing. The wafer surface can be made up of one material or can be a combination of more than one material. Polishing of the top film is affected by the mechanical properties of the films below it. Other factors such as film stress, microstructure and hardness also play an important role in achieving planarization (*11*). Physical parameters such as wafer curvature or size and mounting techniques also affect the wafer polishing. These factors work by the way of influencing the slurry transport and the distribution of the applied load.
2. Slurry: The slurry is a combination of a chemicals and abrasives. These components are selected on the basis of the material being polished as different materials show different chemical interactions. The chemical part of the slurry consists of buffering agents to maintain the pH, oxidizers to increase the oxidation rate, and complexing agents to increase the solubility of the film being polished. The nature and concentration of these chemicals contributes to the etch rate during polishing. The slurry abrasives constitute the mechanical aspect of the slurry by causing abrasion. Chemical and physical properties of these abrasive particles such as nature, size, hardness, and concentration affect the removal rate and the surface damage during polishing.
3. Polishing Pad: The polishing pad supports the wafer being polished while transporting the slurry across its surface. Some of the important pad properties such as fiber structure, compressibility, hardness, modulus, thickness, pore size

and distribution, and chemical durability determine the polishing efficiency as the pad is constantly influenced by the other input parameters.

4. Operating Conditions: These refer to the experimental conditions such as temperature, pressure, platen velocity for the pad and wafer, and slurry flow rate. These parameters again, are controlled in coordination with the other input parameters, mainly for optimizing the process.

1.2.4. Relation between the input and the output variables

As stated earlier, the output variables are the end-representation of the chosen input variables. Extensive research has been done to better understand the relationship between these two sets of variables. To give an example, some of the interaction results are discussed here keeping removal rate as the output parameter of interest.

1. Removal rate, surface defects and abrasive size (*12*): At low pressures and velocities, the removal rate is seen to be independent of abrasive size while at higher values of pressure and velocity, larger abrasive size shows higher removal rates as illustrated in Figure 1.6. Surface defects increase with an increase in the abrasive size. These surface defects are seen in terms of micro-scratches on the wafer surface.
2. Removal rate and slurry flow rate (*13*): At constant values of P x V, with an increase in the slurry flow rate, the removal rate is seen to decrease as shown in Figure 1.7. This has been explained on the basis of a higher flow rate producing more cooling.
3. Removal rate and pad roughness (*14*): Conditioning is an important regeneration process in CMP. In the absence of conditioning, the roughness of the pad is seen

to decrease. As a consequence, the removal rate, which is related to the pad roughness, is also seen to decrease. The results can be seen in Figure 1.8.

1.2.5. Advantages and disadvantages of CMP

CMP is a suitable process to achieve global planarization. Different materials can be planarized using CMP. This implies that a wide range of wafer surfaces may be planarized using CMP. A major advantage of using CMP is that multiple materials can be polished in the same cycle. Use of CMP helps in reducing severe topography, which facilitates the fabrication of IC components with tighter tolerances and design rules. CMP also provides an alternate method to etch metals. This helps in overcoming difficulties associated with etching some metals and alloys and also eliminates the need to plasma etch. More importantly, CMP is a subtractive process and helps in removing surface defects. No hazardous gases are used in CMP process unlike dry etching.

One of the major limitations of the CMP process is that it is a relatively new technology for wafer planarization. Hence, there is not much control over the process variables. The introduction of a new technology implies introduction of new defects, which can affect the die yield. These defects may prove critical for features that are smaller than 0.25μm in size. Since CMP is a relatively new technology, additional development is required to control the process and metrology. For example, at this point it is difficult to control the end point of the CMP process in order to achieve the desired thickness. The CMP process is also expensive due to high cost of equipment and the high maintenance cost from frequent replacement of parts.

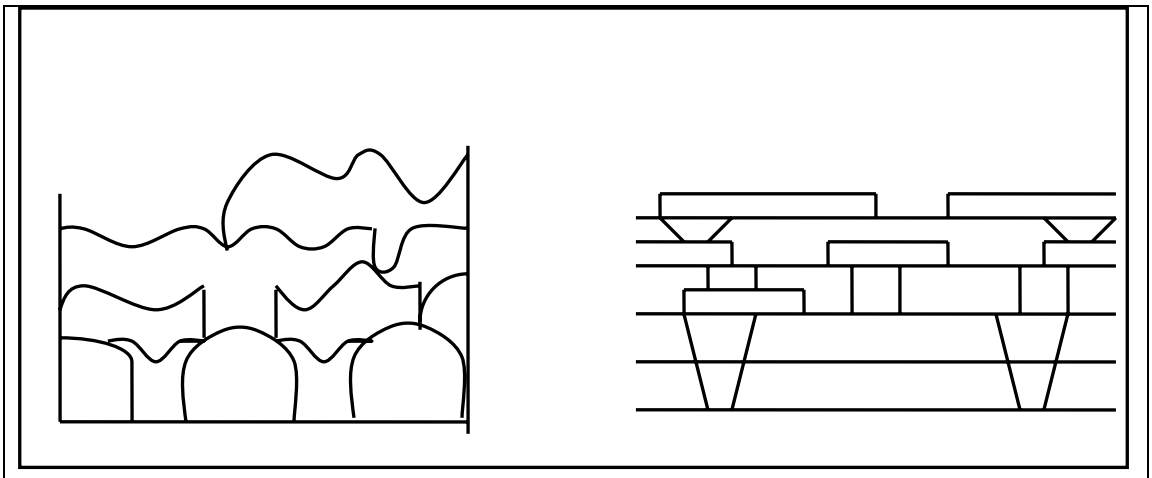

Figure 1.1: Multilevel metallization structure a) Non-planarized; b) Planarized

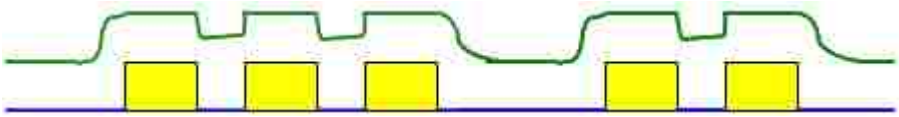

Figure 1.2: Surface smoothing

Figure 1.3: Local planarization

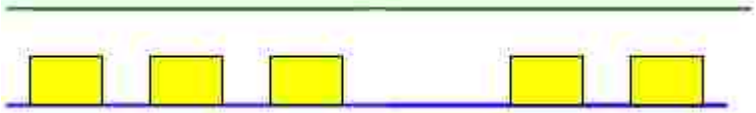

Figure 1.4: Global planarization

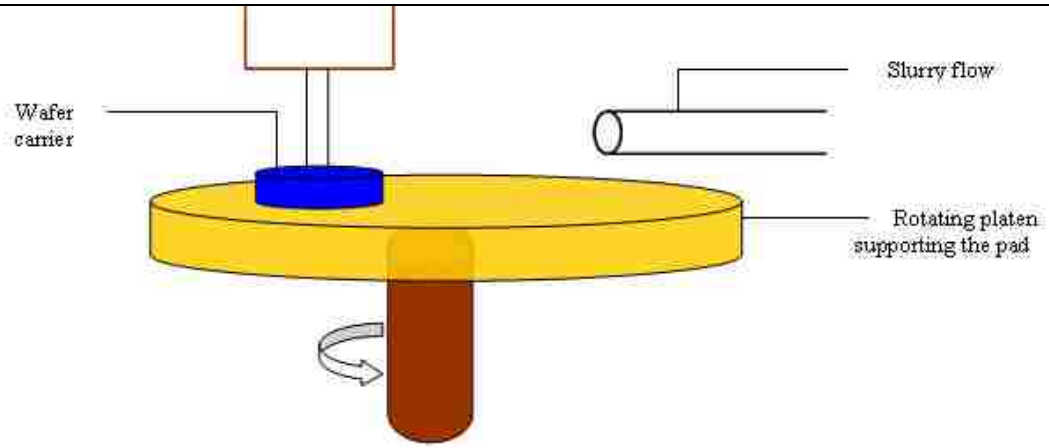

Figure 1.5: Schematic of CMP process

(a)

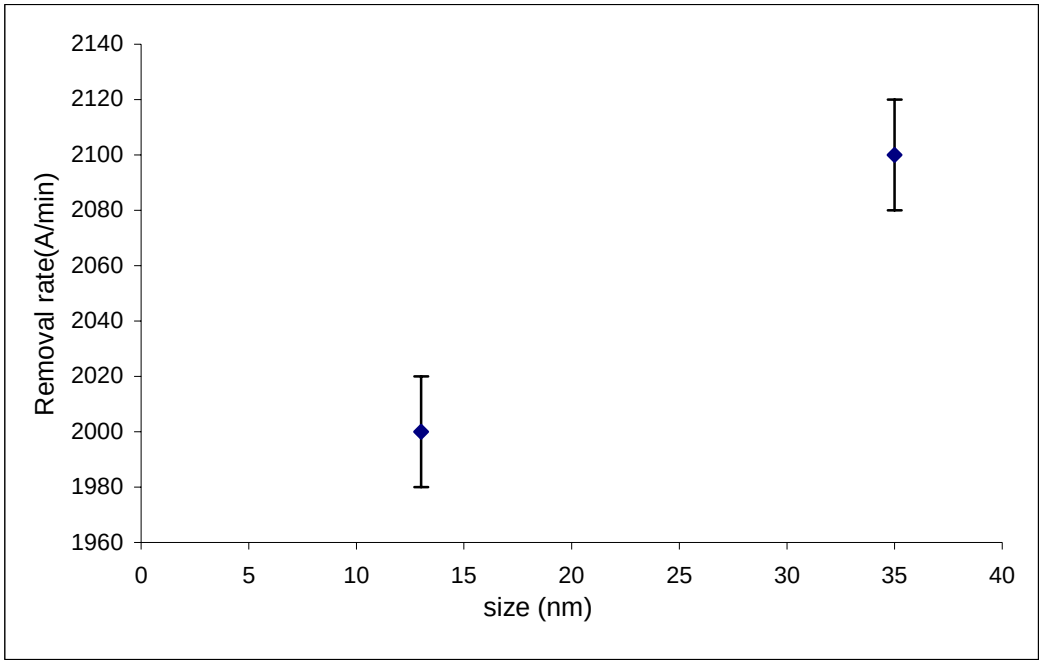

(b)

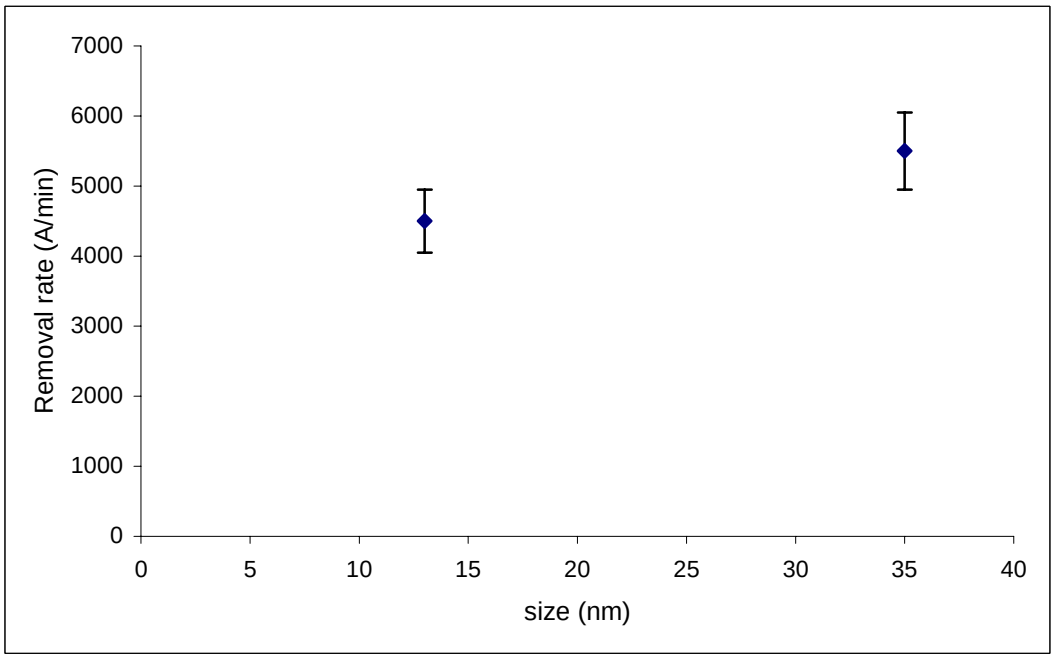

Figure 1.6: Removal rate as a function of abrasive diameter at (a) low and (b) high values of PxV. The data in these figures is from literature (*12*).

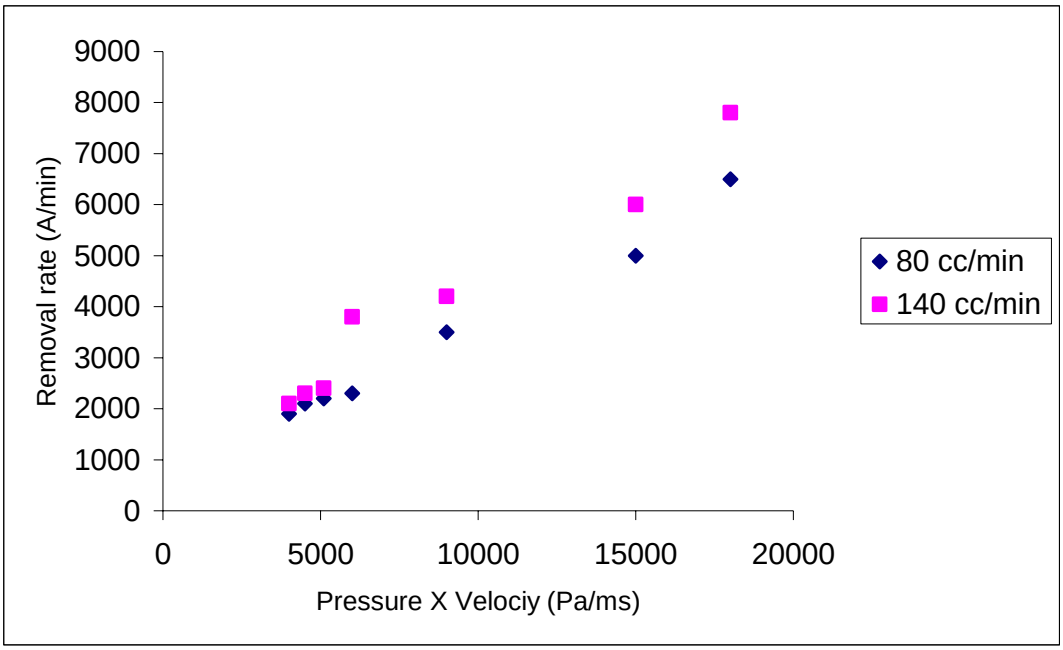

Figure 1.7: Removal rate as a function of PxV showing the effect of slurry flow. The data in the figure is from literature (*13*).

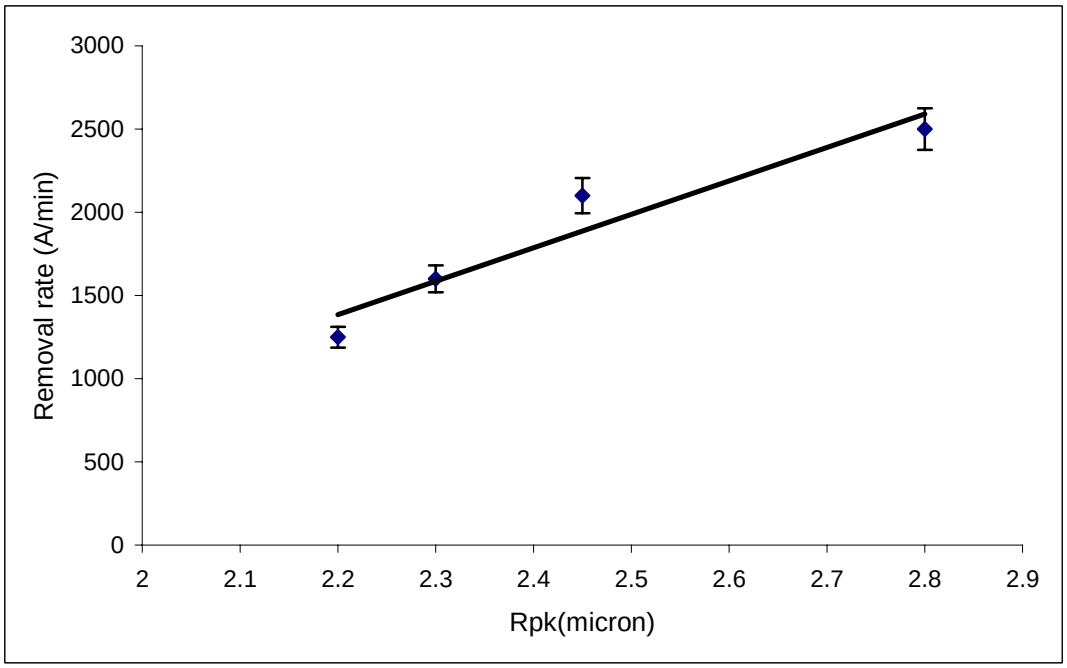

Figure 1.8: Correlation between removal rate and pad roughness. The data in the figure is from literature (*14*).

Chapter 2

Effect of Diamond Size on Conditioning and Polishing in CMP

As discussed in chapter 1, polishing pad is one of the consumables of the CMP process with a direct effect on the output. It acts as the platform on which the polishing is carried out. The pad is made up of a matrix of polyurethane foam with a filler material such as polymer felt (*15*). Mechanical reliability and chemical resistance are essential for the pad to extend the thoroughness of polishing.

2.1. Polishing pad

2.1.1. Pad surface and structure

Polishing pads are generally made up of polyurethane as the chemical properties of this polymer allow modifications to the pad in order to comply with the mechanical needs for the process. Polyurethanes have interesting morphologies. They show contrasting molecular structure of linear elastomers as well as of rigid cross linked polymers.

Based on the microstructure, pads can be divided into four categories (*16*). Type 1 pads typically are polymer impregnated felts. The microstructure of a pad of Type 1 is characterized by non-woven polyester fibers infused with polyurethane. Poromerics form the Type 2 pads and pads of this type display a porous layer on a substrate. Type 3 pads are filled polymer sheet and it is observed that a closed foam structure with macro pores

from mechanical machining occur in these pads. The microstructure of pad of Type 4, which is an unfilled textured polymer sheet, has a non-porous structure. All four types of pads are polyurethane based but are manufactured differently and hence exhibit varied properties. SEM images of these various pads are available in literature (*16*) and clearly show the different microstructure characteristics described above.

2.1.2. Pad properties and polishing performance

The pad properties influence the polishing of the wafer during the CMP process. The material of the pad should be chemically stable and not react with the slurry chemicals. The pad material should be such that it does not get affected by the slurry pH, which may be acidic or alkaline based on the process. The pad should also possess high surface tension in order to promote hydrophilicity for wetting purposes. The hydrophilic nature of the pads aids in the formation of thin film of slurry between the wafer and the pad surface enabling the entire surface of the wafer to be equally subjected to the slurry chemistry. Mechanically, the pad is required to have high strength, acceptable levels of hardness, and good abrasion resistance. These properties can be related to the structure of the pad at the macro and micro levels. At a macro-level, the grooves on the pad surface assist the slurry flow across the surface of the pad and also reduce the potential of hydroplaning. At the micro-scale, the pad roughness and porosity are also seen to influence the removal rate. With water acting as a plasticizer, pad modulus and hardness decrease in wet pads, while there is an increase in the flexibility and ductility (*16*).

The removal rate depends on the pad macro- and micro-structures. The macro-structures refer to the grooves in the pad to prevent hydroplaning. In the absence of the macro-structure, type 4 pads show no removal rates (*17*) while type 3 perforated pads

have shown higher and stable removal rates. Removal rate is also seen to depend on the pad microstructure, which relates to the pad porosity. Type 4 pads, without any porosity show no removal(*18*). Along with the removal rate, the wafer planarity is also affected by the pad properties such as hardness and stiffness (*16, 19-22*). While the stiffness of the pad promotes planarity, the pad hardness is more related to defects in the wafers in the form of scratches. The planarity of the wafer is also seen to increase with the decrease in pad roughness (*23*). Though the pad properties affect the polishing, it is difficult to completely understand the relationships as there are many variables involved in the process.

In order to maintain the pad structure to sustain removal rates, pad conditioning is a basic requirement. Studies have shown that in the absence of conditioning, the removal rates go down. In the absence of a regeneration process, the properties of the polishing pad decline with a marked influence on the material removal rate and polishing uniformities. During polishing, the pad surfaces get glazed. This glazing reduces the pad porosity and roughness, which affects the slurry transport and the contact area between the pad and the wafer. All these factors result in reducing the efficiency of the CMP process. In order to achieve higher removal rates and planarity, regeneration of the pad is a necessity. This is done by a process known as conditioning where the pad surface is abraded to open up the clogged pores and break the glazed areas.

2.2. Pad conditioning

As discussed earlier, pad conditioning is an important process to restore the pad properties that deteriorate over time during polishing. The surface interactions involved

in the process of polishing are influenced by the pad texture resulting from conditioning. The process of conditioning is used to:

1. maintain the roughness of the pad and promote effective slurry distribution
2. remove unwanted products after polishing.

Various pad conditioning methods have been used to improve the pad properties and stabilize the removal rates. The most effective method found was using diamond as the abrasive material. The properties of the conditioner such as diamond density and diamond mounting play a major role. The other input variables for the conditioning process include parameters such as conditioning downforce and relative speed of rotation (rpm) of the pad platen and the conditioner.

The process of conditioning can be quantified in terms of material removal rate (MRR), pad roughness, and wear of pad. It has been found that a pad conditioned before the first polished wafer doubled the removal rate compared to the unconditioned pads. A repeated conditioning also showed a stable removal rate (*16*). The conditioning maintains the removal rate by maintaining the asperity height and density on the pad surface (*24*). Though the properties of the glazed pad improve with conditioning, there exists a side effect of pad wear. An uneven pad wear results in uneven distribution of the pressure affecting the planarization uniformity and removal rate.

During the process of conditioning, the conditioner disk rotates about its axis and simultaneously moves linearly towards and away from the center of the pad for a uniform conditioning of the pad surface. The conditioning time has to be adjusted so as to maintain the pad thickness. Kinematic equations have been used to model the conditioning processes (*25*).

2.2.1. Conditioners

Conditioners or conditioning disks are used as a medium to present the conditioning abrasive to the pad surface in a way that the desired conditioning effects are achieved. The abrasives present in the slurry are extremely hard. In order to prevent wear of the conditioners due to the presence of such abrasives on the pad, it is necessary to use diamonds as abrasives on the conditioner. The conditioning disks are available in a variety of configurations ranging from solid disks to open patterns. A variety of ways exist to bind diamonds to the surface of conditioning disks. The manner in which diamonds are bound to the surface of the conditioning disks has a bearing on the disk lifetime and the extent of damage caused to wafers due to scratches. The shape of the abrasive as it protrudes from the surface may be controlled by the choice of the diamond. All these factors affect either the conditioning process or the life of the conditioning disk. The conditioning effect is influenced by the profile of the diamond, density of the diamond, the downforce, and the shear velocity. The diamond may either be placed in an orderly fashion across the conditioner disk or they may be randomly placed on the surface of the conditioning disk. Besides the abrasive shape, the effect of the conditioning profile is dependent on the degree of protrusion of the diamond from the conditioning disk. If the degree of protrusion is high, a large torque is experienced by the adhesive mounting surface bond which may lead to higher instability.

2.3. Research focus

Extensive work (*26-29*) has been done in order to understand the effect of conditioning on the polishing pad and polishing rates. As discussed in the previous section, the diamond abrasives present on the conditioning disks play a major role. Therefore, effect of diamond grit size and conditioning force on the polishing pads has been investigated in literature. For example, interferometry analysis was conducted on IC 1000 pads that were conditioned by 100-grit and 325-grit diamond conditioners under varying force and incremental loading. Larger diamonds were seen to create a rougher pad surface under greater force. The other important observation that was made was with regards to the decay lengths. It was concluded that wet pads showed higher decay lengths than the dry pads (*30*).

In contrast to the literature studies, the objective of this research is to investigate the effect of diamond abrasive size under the same loading conditions. The goal is to understand the impact on the pad morphology and subsequently the effect of conditioning on the polished wafer. In addition, in this thesis the effect of duration of conditioning is explored in a systematic manner.

2.4. Experimental setup

The results presented in this chapter focus on the effect of different abrasive sizes on the pad morphology. The experiments were conducted on a bench top CMP tester manufactured by CETR, Inc. (Figure 2.1). The CMP process on this bench top polisher closely imitates the large wafer fabrication production processes in industries. As can be seen from Figure 2.1, the bench top CMP tester consists of an upper platen, which can

hold a two inch wafer. The upper platen itself is held in place by a carriage. The carriage rotates about its own axis at a set rpm (typically 100-150) during polishing. A strain gauge force sensor (0-200 N) is present in the carriage that records both vertical and friction forces. This helps in monitoring the coefficient of friction during the process. An acoustic emission (AE) sensor is also present in the carriage that has a frequency range of 0.5 to 5 KHz. An AE event occurs whenever there is a rapid release of elastic energy within any material. This rapid release of energy propagates an elastic wave that can be detected and analyzed using appropriate sensors. In the case of the bench top CMP process, the AE sensor helps in capturing the acoustic emission from the contact of rubbing surfaces which is an important parameter of friction and wear.

The CMP tester also consists of a lower platen on which a six inch polishing pad is mounted. The lower platen rotates at a set rpm during the process and the set rpm ranges from 100 to 200. The slurry flows over the pad during the polishing process. Pipes are provided for the inflow and outflow of the slurry. The bench-top tester is controlled through a computer.

2.5. Conditioning experiments

Towards the objective of evaluating the effect of abrasive size on the pad morphology, three parameters were varied. These parameters include abrasive size, time of conditioning, and rotational speed of the polishing pad. The polishing pad used was IC 1000 and sub-pad used was SUBA IV. Deionized (DI) water was used as fluid in these experiments.

Five different sizes of diamond abrasives ranging from 0.25μm to 100μm were chosen to carry out the conditioning on the commercially available polishing pad. The different sizes of diamond abrasives used were 0.25μm, 2μm, 8μm, 68μm, and 100μm. Though all these conditioners appear alike to the naked eye, the different diamond sizes can be clearly distinguished in corresponding SEM images as seen in Figure 2.2 through Figure 2.11. In order to evaluate the influence of abrasive size on pad morphology, conditioning was carried out for four different times: five, ten, fifteen, and twenty minutes. Thus, for each size of abrasive, four different experiments were conducted. In addition, each experiment was conducted at two rotation speeds (150 rpm and 200 rpm) of the pad. The results of these experiments are discussed in the next section.

2.6. Results of conditioning experiments

In these experiments, in-situ coefficient of friction was monitored. The pad surfaces after conditioning were characterized using SEM, AFM, Dynamic Mechanical Analysis (DMA) and profilometry. The pads were evaluated with respect to their morphology, roughness, and storage modulus. The hypothesis in these experiments is that the size of the diamond abrasives affects the degree of abrading as long as the conditioning time remains the same.

2.6.1. Pad morphology

Figure 2.13 shows the morphology of the pad conditioned with an abrasive size of 0.25μm. In this case the pad has been conditioned for five minutes at 150 rpm. From this image, it can be observed that the pad morphology remains relatively the same as compared to the pad morphology prior to conditioning as in Figure 2.12. Similarly,

Figure 2.14 shows the morphology of the pad having been conditioned with an abrasive size of 100µm. In this case, the pad has been conditioned for five minutes at 150 rpm. On comparing the morphology of the conditioned pad to the morphology of the pad prior to conditioning, it can be seen that significant abrasion has occurred. On comparing Figure 2.13 and Figure 2.14, it can be inferred that for the same conditioning time and the same rotation speed, the degree of abrasion is significantly more for a higher abrasive size.

Figure 2.15 to Figure 2.19 show the morphology of the pads that have been conditioned for five minutes using abrasives with sizes of 0.25µm, 2µm, 8µm, 68µm, and 100µm at 150 rpm. These images are an indication that as the abrasive size increases, the degree of abrading increases. Figure 2.20 to Figure 2.24 show the pads conditioned for five minutes at 200 rpm. These results show the same trend as shown by pad morphologies conditioned at a lower rpm. On comparing the two sets of conditioning results, it can be concluded that for same conditioning time, the rpm does make a significant difference on the pad morphologies. However, since five minutes may not be enough to draw conclusions, the conditioning process was carried out for the same abrasive sizes mentioned above but for different times.

Having conducted the conditioning experiment for five minutes, the second step is to conduct the conditioning experiment for times of 10, 15, and 20 minutes at 150 and 200 rpm. Figure 2.25 to Figure 2.29 show the morphology of the pad that has been conditioned for twenty minutes for abrasive sizes of 0.25µm, 2µm, 8µ, 68µm, and 100µm at 150 rpm. On comparing Figure 2.15 and Figure 2.25, it can be seen that as the time of conditioning increases from five to twenty minutes, the degree of abrading is

significantly more. The same is the case with the 100μ abrasive size. This result can be inferred by comparing Figure 2.19 and Figure 2.29.

Figure 2.30 through Figure 2.34 show the pad conditioned for twenty minutes at 200 rpm. On comparing these results to the previous conditioning results, the maximum pad abrasion is seen in this set of results because of the combination of higher platen speed and longer abrasion time. The pad surfaces conditioned for twenty minutes at 200 rpm show a more uniform abrasion.

The smaller abrasive do not show much change in the pad morphology for a short duration but with longer conditioning time, pad abrasion is seen clearly whereas the effect of bigger abrasives becomes clear even with a short conditioning time. Again, a higher rpm shows more pad abrasion than a lower rpm. Though, there does not exist a wide gap in the rpm values chosen here, the difference becomes prominent for longer conditioning duration.

2.6.2. Pad wear

The reduction in thickness of the pad as the conditioning proceeds is defined as pad wear. The conditioner has to maintain constant contact with the pad throughout the conditioning process. In order to maintain constant contact, the carriage automatically comes down by the same amount by which the thickness of the pad decreases. The distance by which the carriage travels downward is a measure of the amount of wear in the pad.

Figure 2.35 and Figure 2.36 show plots of the amount of pad wear against time for different abrasive sizes at a pad rotation speed of 150 and 200 rpm. From Figure 2.35 at 150 rpm, it is observed that for larger abrasive, the amount of wear in the pad is higher

than at smaller abrasive. For example, for an abrasive size of 100µm the amount of wear at five minutes is 0.018µm whereas for an abrasive size of 0.25µm, the amount of wear is 0.006µm. As the time for conditioning increases, the amount of wear also increases. For example, when the abrasive size is 100µm, the amount of wear is 0.026µm for a conditioning time of 10 minutes, and 0.03µm for a conditioning time of 20 minutes. Similarly, when the abrasive size is 0.25µm, the amount of wear is 0.008µm for a conditioning time of 10 minutes, and 0.01µm for a conditioning time of 20 minutes. The same trend is observed in Figure 2.36, when the pad rotation speed is set at 200 rpm. However, the amount of wear is more at 200 rpm as compared to the amount of wear at a rotation speed of 150 rpm. For example, at 150 rpm, the amount of wear when using 8µm abrasive size for a conditioning time of 20 minutes is 0.015µm, whereas at 200 rpm it is 0.016µm. As bigger abrasives abrade the pad to a higher degree than the smaller abrasives, the pad wear caused due to this abrasion is also more in the case of bigger abrasives. Higher the pad wear, shorter is the pad life. An uneven pad wear also results in uneven slurry transport and non-uniform polishing.

2.6.3. Coefficient of friction

Having looked at the pad morphology and pad wear, the next step is to evaluate the coefficient of friction resulting from the different abrasive sizes. During the conditioning process, the lower platen exerts a normal force equivalent to the downward force experienced by the pad. There is a shear force also present between the pad and conditioner. The coefficient of friction between the pad and the conditioner is computed as a ratio of the shear force to the normal force.

Figure 2.37 and Figure 2.38 show the plots of coefficient of friction against time for the conditioning runs at 150 and 200 rpm respectively. From the plots it is observed that as the abrasive size increases, the coefficient of friction increases. For example, in Figure 2.37, for an abrasive size of 100μm, the COF is 0.633 at 150 rpm when the time for conditioning is five minutes, whereas, the COF is 0.32 for an abrasive size of 0.25μm. Similarly, for 100 μm abrasive size, when the time for conditioning is 20 minutes, the COF is 0.645, whereas for a conditioning size of 0.25μm the COF is 0.47.

Figure 2.38 shows a plot of coefficient of friction against time for the conditioning run at a pad rotation speed of 200 rpm. In this case as well, the coefficient of friction for larger abrasive size is generally higher than the coefficient of friction for a smaller abrasive size.

As discussed above, pad wear is more at higher pad rotation speeds than at lower pad rotation speeds and so there is a decrease of shear force between the pad and the conditioner. This further implies that the coefficient of friction should decrease as the pad rotation speed increases as seen in the plots. For an abrasive size of 100μm, the average coefficient of friction at 150 rpm is 0.624 whereas at 200 rpm the average coefficient of friction is 0.589. Similarly, when the abrasive size is 2μm, the average COF at 150 rpm is 0.44 whereas at 200 rpm, the COF is 0.40.

2.6.4. Pad roughness

The roughness of the pad affects the removal rate as the wafer being polished comes in direct contact with the rough surface of the pad (31). Having evaluated the coefficient of friction, the next step is to evaluate the roughness of the pad. This was done using a contact mode profilometer with a stylus of radius 12μm. A standard scan was

conducted over a 50μm scan length. There were five measurements for each pad. The average roughness measurements of each pad are plotted against the abrasive size of the conditioner used for that pad.

Figure 2.39 shows the plot of pad roughness with respect to time for different abrasive sizes at 150 rpm. It can be seen from the plot that the roughness increases with time. For the smaller abrasive sizes of 0.25μm, 2μm and 8μm the increase in pad roughness with time is not much. For a conditioning time of 5 minutes, the pad roughness values were 0.775, 1.03 and 1.26 μm for abrasive sizes of 0.25μm, 2μm and 8μm, respectively. For a conditioning time of 20 minutes, the roughness values for 0.25μm, 2μm and 8μm abrasives are 1.23, 1.28 and 2.05μm, respectively. The conditioning with bigger abrasives results in higher roughness compared to the smaller abrasives. For 15 minute conditioning, the pad roughness value for 68μm and 100μm are 2.26 and 2.38μm, respectively. As can be seen from the plot, for a conditioning run of 20 minutes, the pad roughness for 68μm is still increasing while for 100μm the pad roughness value seems to decrease. For 100μm abrasive for 20 minutes, as the pad abrasion is relatively high, this could result in rupturing of the pad surface rather than just restoring the roughness.

Figure 2.40 shows the plot of pad roughness with respect to time for different sizes at 200 rpm. On comparing the roughness values obtained at 200 rpm with those at 150 rpm, it is observed that the pad roughness values at 150 rpm are higher than those at 200 rpm. This can be because that at a higher rotational speed of 200 rpm, the pad does not get abraded uniformly.

2.6.5. Dynamic Mechanical Analysis

Having investigated the roughness of the pads, dynamic mechanical analysis was conducted to evaluate the relation between structure and properties of the pad. DMA is used to study the mechanical properties of polymers and analysis is based on the principle that viscoelastic materials dissipate stored mechanical energy when deformed (*32*). DMA studies on CMP pads have been performed to understand the structure property relations. The storage and loss modulus give an insight into the elastic and viscous nature respectively of the viscoelastic materials. The ratio of these two moduli is given by tan δ. This ratio is useful during the characterization of polymers since it is related to the material's ability to dissipate energy in the form of heat (*33*).

For this experiment, the pad that was conditioned with 100μm abrasive size conditioner for 20 minutes at a pad rotation speed at 200 rpm was used. Samples (35 mm X 15 mm) were cut from each pad. In order to facilitate efficient clamping of the pad coupon to the holder, the bottom glue layer was scrubbed off of the coupon. The data was obtained on a TA Instruments DMA 2980 (New Castle, DE) at 4^{o}C with an isothermal time of one minute per increment starting from room temperature (30^{o}C) and going up to 80^{o}C. A single cantilever clamp was used in the flexural mode with amplitude of 3μm. The data was collected at six different frequencies; 0.6, 6, 12, 30, 60, and 100 Hz. As the pads conditioned for twenty minutes at 200 rpm showed the maximum change in terms of pad morphology, pad wear and pad roughness, DMA was carried out for this set of conditioned pads.

Figure 2.41 and Figure 2.42 show the plots of storage modulus of the pad against temperature at 30Hz and 100Hz respectively. The plot shows the storage modulus of pads

conditioned with conditioners of abrasive sizes 0.25µm, 2µm, 68µm, and 100µm. As can be seen from the plot, the storage modulus does not vary much for the different pads. For example, the storage modulus of the pad conditioned with 2µm abrasive size conditioner is higher than that of the pad conditioned using a 0.25µm conditioner. However, for the pad conditioned using conditioner of 68µm abrasive size, the storage modulus was higher compared to all other pads. Excessive wear of the pad conditioned using 100µm abrasive conditioner may have resulted in a lower storage modulus.

The pad conditioned with 8µm seems to show abnormally lower storage modulus compared to the other conditioned pads. The number of punched holes in this sample were about 18 while in the other samples, the number of holes were about 12-14. So, the sample used for testing was less stiff compared to the others.

2.7. Polishing experiments

In this experiment, the same CETR bench-top tester was used as in the conditioning experiments. Polishing differs from conditioning in that the upper platen holds a wafer instead of a conditioner. The object of interest is the wafer being polished rather than the pad as in conditioning. The conditioned pad acts as a polisher in the presence of slurry and smoothens the wafer. Hence, the pad plays an important role in the outcome of the polishing process. Since the pad morphology is affected by the abrasive size, the abrasive size indirectly affects the surface of the wafer. Hence, the set of experiments described here investigate the affect of using pads of different morphologies that resulted from different abrasive size conditioners on the surface of the wafer.
As mentioned earlier, the objective of these experiments is to evaluate the effect of abrasive size on the surface of the polished wafer. In order to do so, three different

abrasive sizes were used; 8µm, 68µm, and 100µm. The polishing pad used was IC 1000 and sub-pad used was SUBA IV. The slurry used during polishing was Cabot 5001, which is commercially available. The results obtained for these experiments are discussed in the next section.

2.8. Results of the polishing experiments

After conducting the experiments, an optical microscope was used in order to obtain optical images of the polished wafers to evaluate surface defects such as micro-scratches. The topography of the wafer was evaluated using an AFM. In a manner similar to the conditioning experiments, the in-situ coefficient of friction was monitored. SEM images of the pad were taken after polishing in order to evaluate the pad morphology.

2.8.1. Optical images of the polished wafer

For the polishing experiment, having polished a wafer using a pad, the pad was conditioned again before reusing it for the next wafer. This process was repeated for three wafers. Figure 2.43 and Figure 2.44 show the optical images of the first and third wafers that were polished using pads conditioned by an 8µm abrasive size conditioner. Similarly, Figure 2.45 and Figure 2.46 show the optical images of the first and third wafers that were polished using pads conditioned by a 68µm abrasive size conditioner. Optical images of the first and third wafers polished using a pad conditioned by 100µm abrasive size conditioner are shown in Figure 2.47 and Figure 2.48.

On comparing images of the first wafer polished by the pads conditioned using the three different abrasive size conditioners, it is observed that the pad conditioned using the 100µm abrasive size conditioner produces a large number of scratches on the wafer.

A lot of scratches developed are in clusters and the scratches are small in size. Similarly, when the pad conditioned using a 68µm conditioner is used, scratches are produced in clusters. However, the number of scratches in each cluster is relatively less than that when using the 100µm conditioner. The scratches themselves are relatively longer when compared to those produced by the 100µm conditioner. The pad conditioned using the 8µm conditioner produces relatively longer scratches when compared to the scratches produced by the pads conditioned using the 68µm and 100µm conditioners and unlike the other wafers, the scratches are isolated.

From the optical images obtained for the third wafer polished by the pad conditioned using the 100µm abrasive size conditioner, it is observed that the pad produces less number of scratches on the third wafer as compared to the first wafer. Similarly, the pad conditioned using the 68µm abrasive size conditioner produces less number of scratches on the third wafer as compared to the first wafer. However, the pad conditioned using the 8µm abrasive size conditioner produces relatively the same number of scratches on the first and third wafers.

2.8.2. Evaluation of topography

Atomic Force Microscope was used to evaluate the wafer and pad topography. For this purpose, a Digital Instruments Dimension^{TM} 3100 AFM was used and operated at 256 Hz frequency of the cantilever.

Wafer Topography: For this experiment, the roughness measurements were taken at different points across the surface of the wafer from the center of the wafer to its edge. Figure 2.49 and Figure 2.50 show the AFM images of the first and third wafers that were polished using pads conditioned by an 8µm abrasive size conditioner. Similarly, Figure

2.51 and Figure 2.52 show the AFM images of the first and third wafers that were polished using pads conditioned by a 68µm abrasive size conditioner. AFM images of the first and third wafers polished using a pad conditioned by 100µm abrasive size conditioner is shown in Figure 2.53 and Figure 2.54.

On comparing the AFM images of the first and third wafer polished using a pad conditioned with a 100µm abrasive size conditioner, it can be observed that the first wafer is rougher. The roughness value of the third wafer is 34 nm whereas the roughness of the first wafer is 38 nm. Similarly, when using a pad conditioned with an 8µm abrasive size conditioner, the first wafer has a roughness of 83 nm while the third wafer has a roughness of 70 nm.

On comparing the roughness values of the wafers polished using each of the three pads, it is observed that the roughness value of the wafer polished by the pad conditioned using the 100µm conditioner is significantly less compared to the wafers polished using the other two pads. This implies that it is possible to achieve more planarization using the pad conditioned with the 100µm abrasive size conditioner.

Pad Topography: The AFM images of the pads used in polishing the wafers are shown in Figure 2.55 to Figure 2.57 for the abrasive size of 8µm, 68µm and 100µm respectively. On comparing the images of the different pads used in the polishing process, it is observed that the pad conditioned using the 100µm abrasive size conditioner has higher roughness values as compared to the other two pads.

2.8.3. Pad morphology

Figure 2.58 shows the morphology of the pad conditioned with an abrasive size of 8µm. As can be seen, this pad does not exhibit uniform conditioning. Figure 2.59 shows

the morphology of the pad conditioned with an abrasive size of 68µm and Figure 2.60 show the pad conditioned with a 100µm conditioner. From these images, it can be observed that the higher abrasive size conditions the pad more uniformly.

2.8.4. Coefficient of friction

Having looked at the pad morphology, the next step was to evaluate the COF resulting from using different abrasive sizes. Figure 2.61 to Figure 2.63 show plot of coefficient of friction against time for the polished wafer conditioned on pad with abrasive size of 8µm, 68µm and 100µm. For an abrasive size of 8µm, the COF is 0.6045. COF for an abrasive size of 68µm is 0.2690 as seen in Figure 2.62. For an abrasive size of 100µm, Figure 2.63 shows that the COF is 0.407. As can be seen, the COF plots for 68µm and 100µm seem to follow the same pattern with high variation in the beginning and then the variations are reduced with time. For 8µm abrasive, COF plot shows increasing variations with time. This implies that a polishing run of three minutes may not be sufficient for this abrasive size. If the process were allowed to run longer, the COF value may decrease.

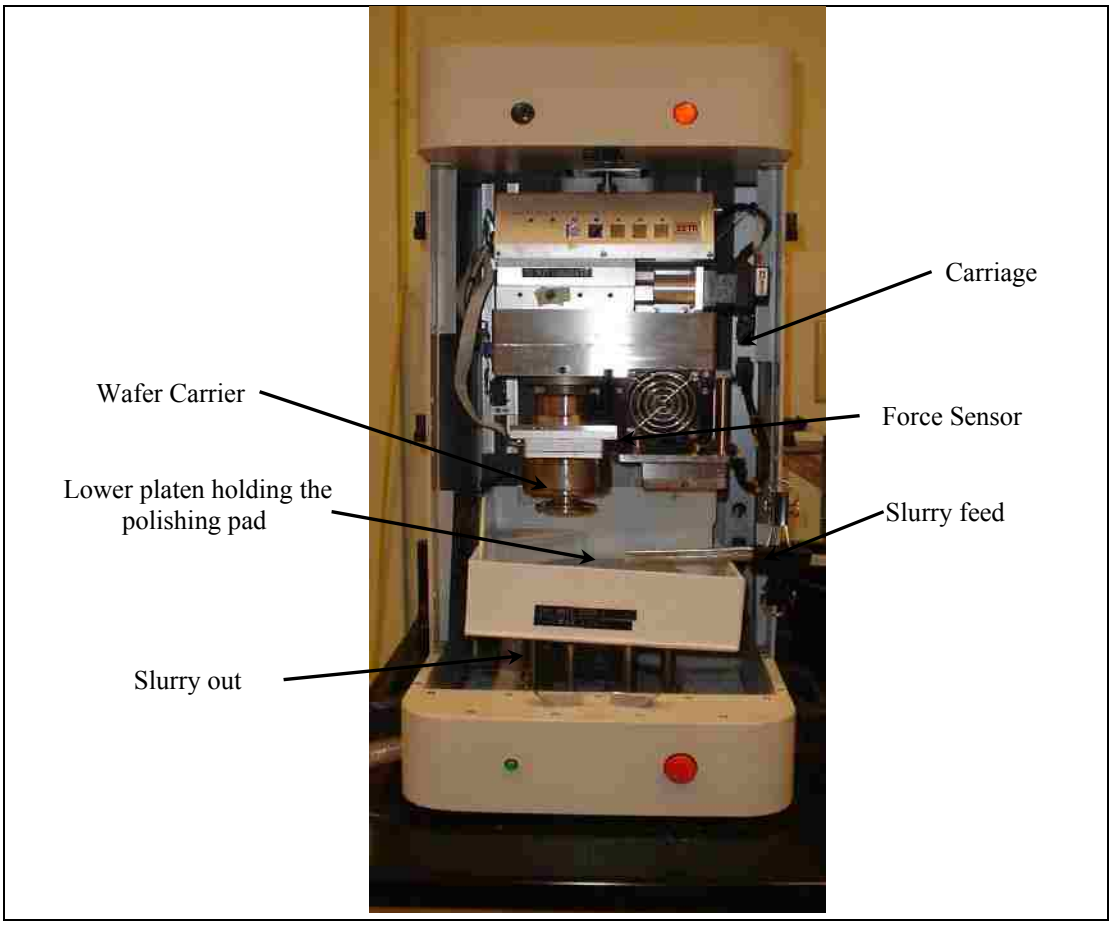

Figure 2.1: CETR bench top tester

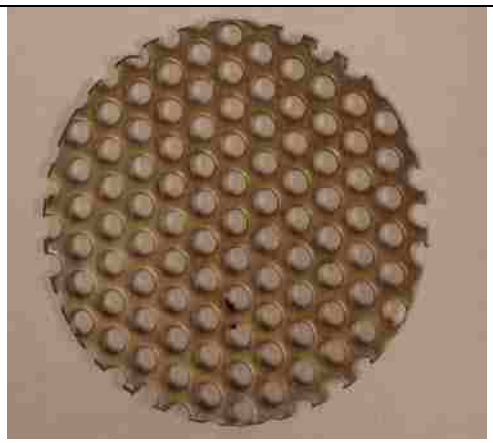

Figure 2.2: Photograph of a 0.25µm abrasive conditioner

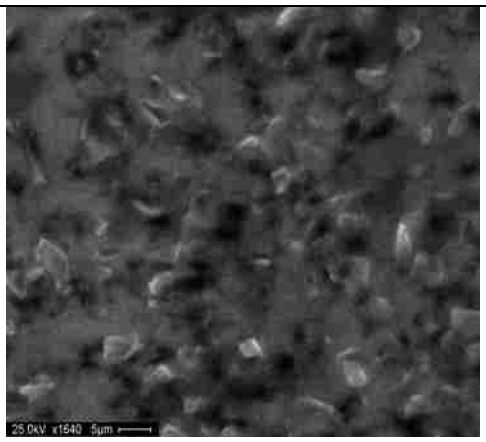

Figure 2.3: SEM image of a 0.25µm abrasive conditioner

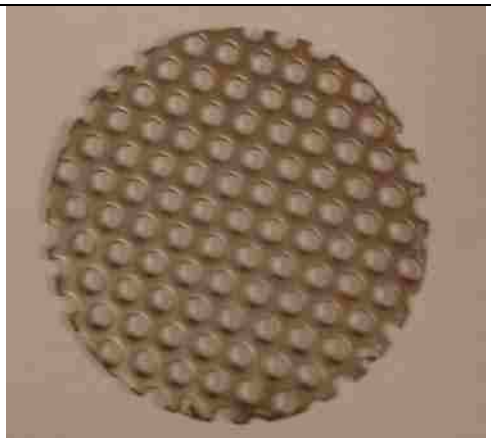

Figure 2.4: Photograph of a 2µm abrasive conditioner

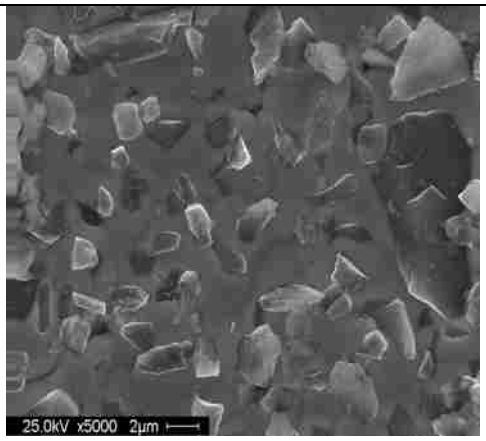

Figure 2.5: SEM image of a 2µm abrasive conditioner

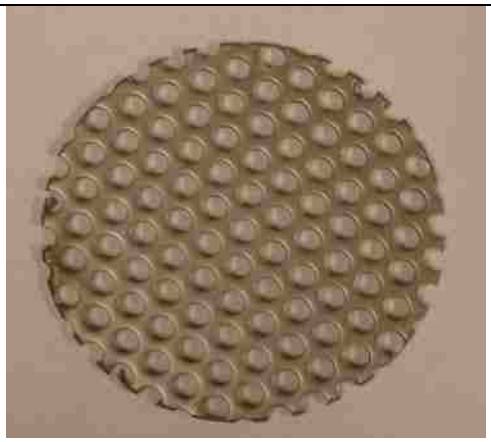

Figure 2.6: Photograph of a 8µm abrasive conditioner

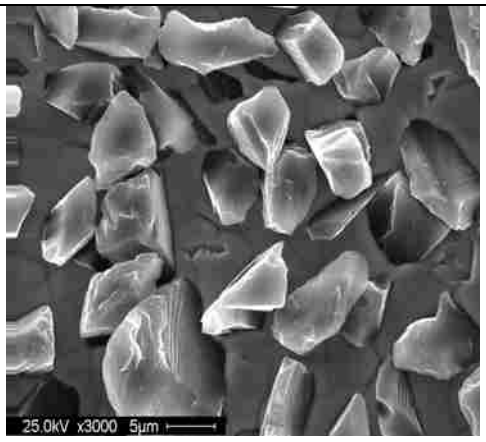

Figure 2.7: SEM image of a 8µm abrasive conditioner

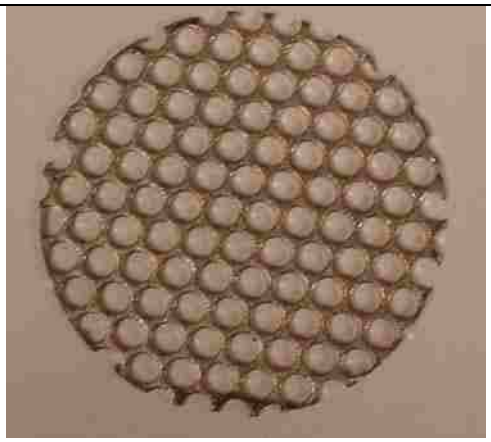

Figure 2.8: Photograph of a 68µm abrasive conditioner

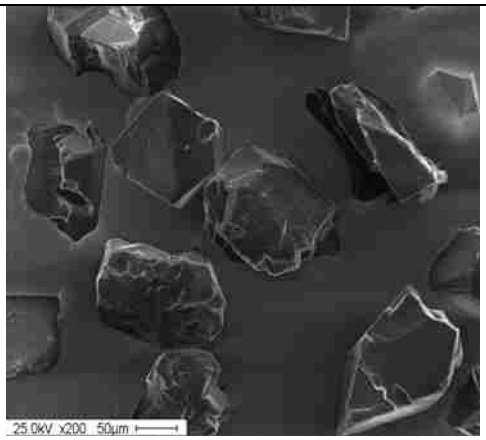

Figure 2.9: SEM image of a 68µm abrasive conditioner

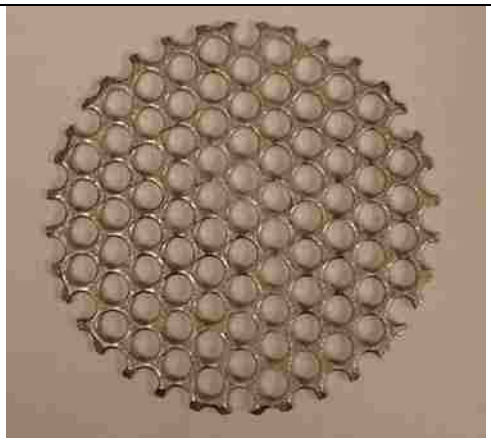

Figure 2.10: Photograph of a 100µm abrasive conditioner

Figure 2.11: SEM image of a 100µm abrasive conditioner

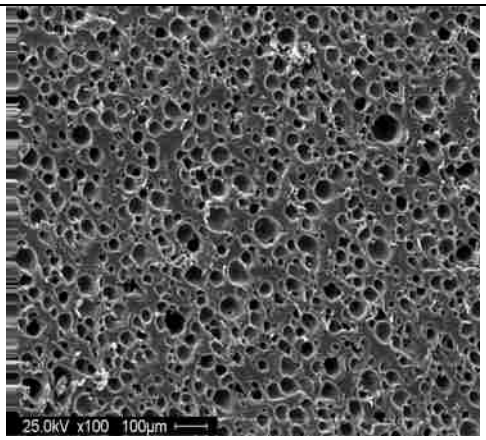

Figure 2.12: SEM image of a fresh pad

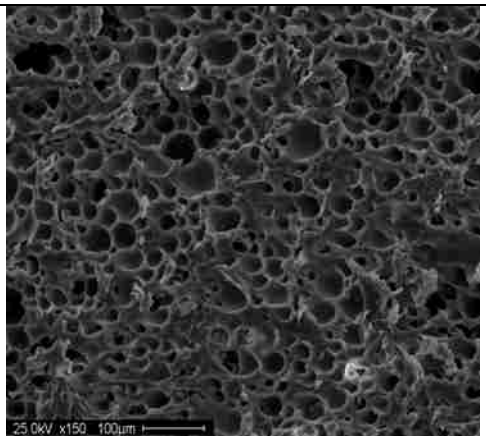

Figure 2.13: SEM image of pad conditioned using 0.25µm abrasive

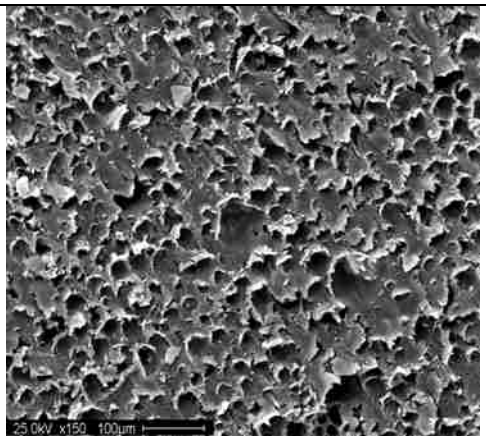

Figure 2.14: SEM image of pad conditioned using 100µm abrasive

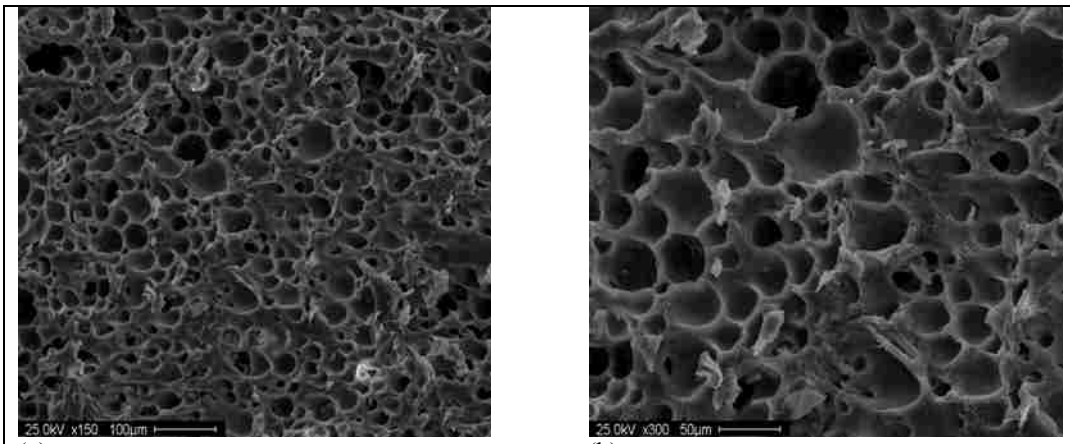

(a) (b)

Figure 2.15: SEM images of pad conditioned with 0.25µm abrasive for 5 min at 150 rpm at two different magnifications (a)150X (b)300X

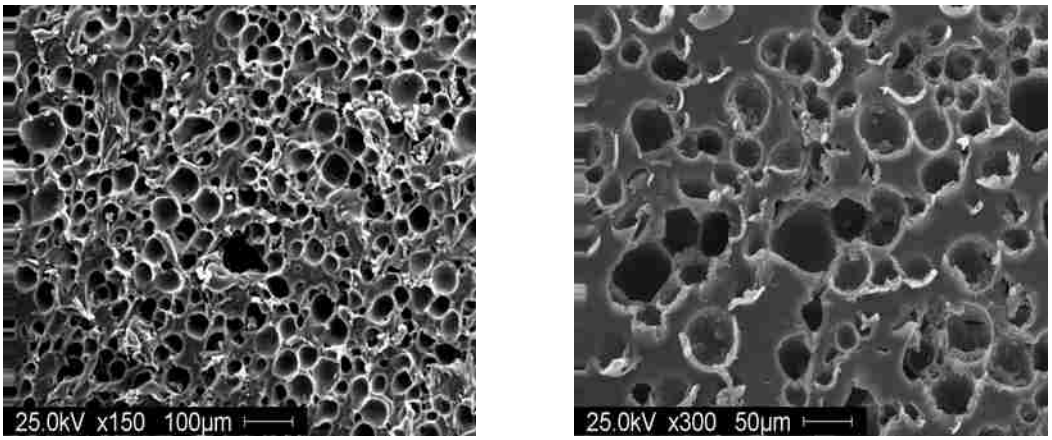

(a) (b)

Figure 2.16: SEM image of pad conditioned with 2µm abrasive for 5 min at 150 rpm at two different magnifications (a)150X (b)300X

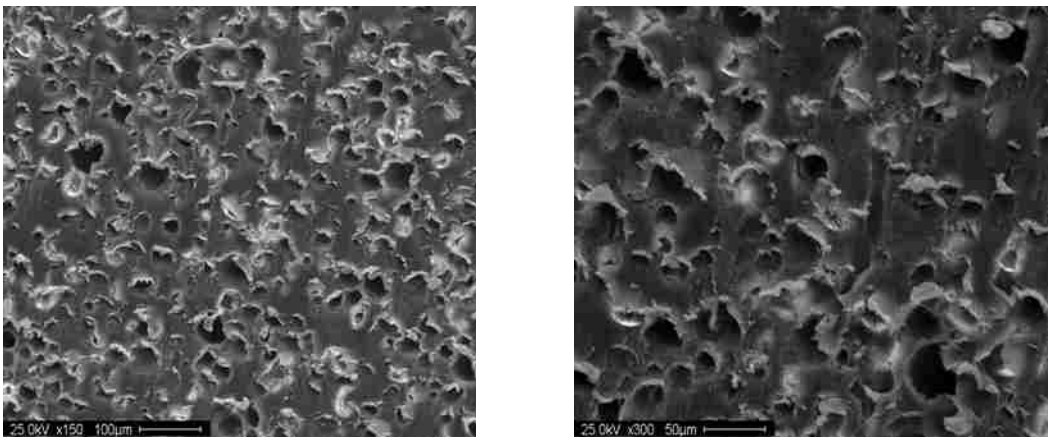

(a) (b)

Figure 2.17: SEM image of pad conditioned with 8µm abrasive for 5 min at 150 rpm at two different magnifications (a)150X (b)300X

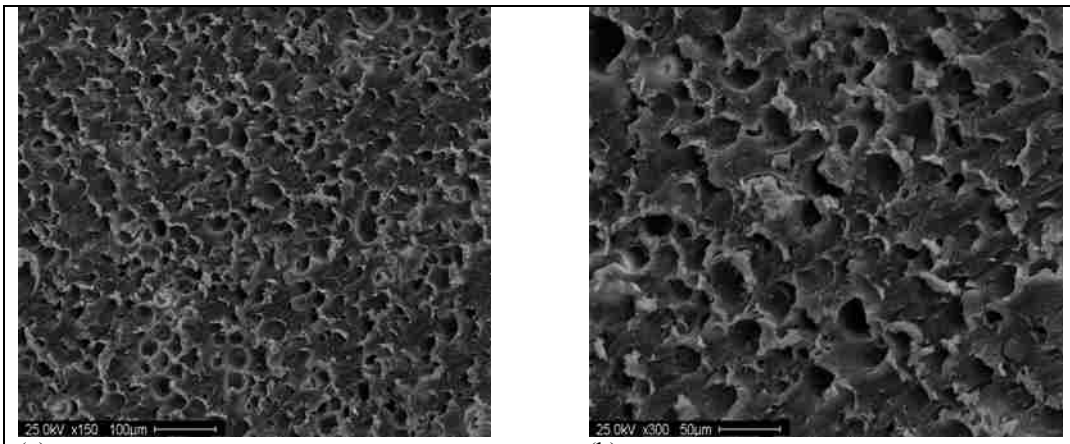

(a) (b)

Figure 2.18: SEM image of pad conditioned with 68µm abrasive for 5 min at 150 rpm at two different magnifications (a)150X (b)300X

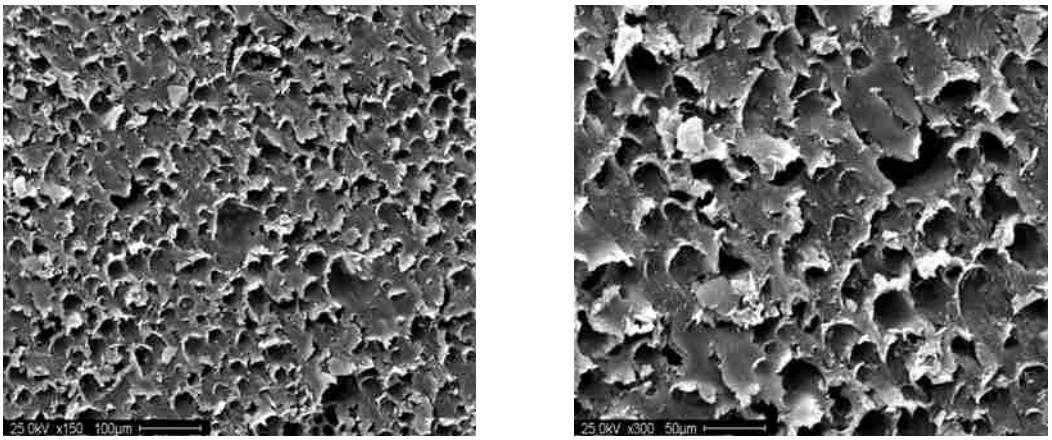

(a) (b)

Figure 2.19: SEM image of pad conditioned with 100µm abrasive for 5 min at 150 rpm at two different magnifications (a)150X (b)300X

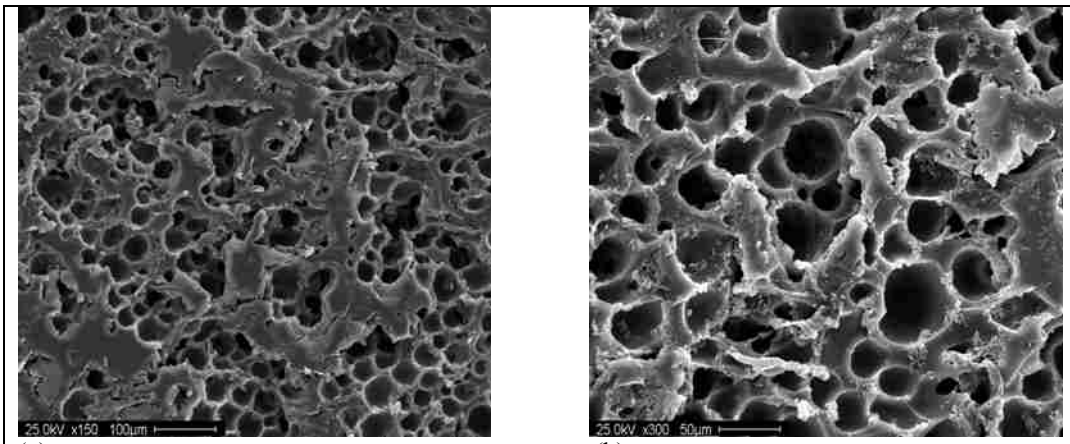

(a) (b)

Figure 2.20: SEM image of pad conditioned with 0.25µm abrasive for 20 min at 150 rpm at two different magnifications(a)150X (b)300X

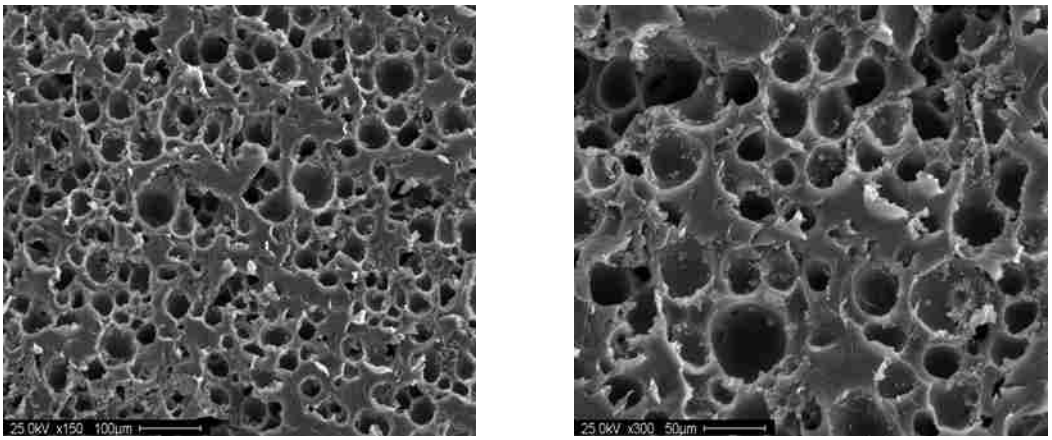

(a) (b)

Figure 2.21: SEM image of pad conditioned with 2µm abrasive for 20min at 150 rpm at two different magnifications (a)150X (b)300X

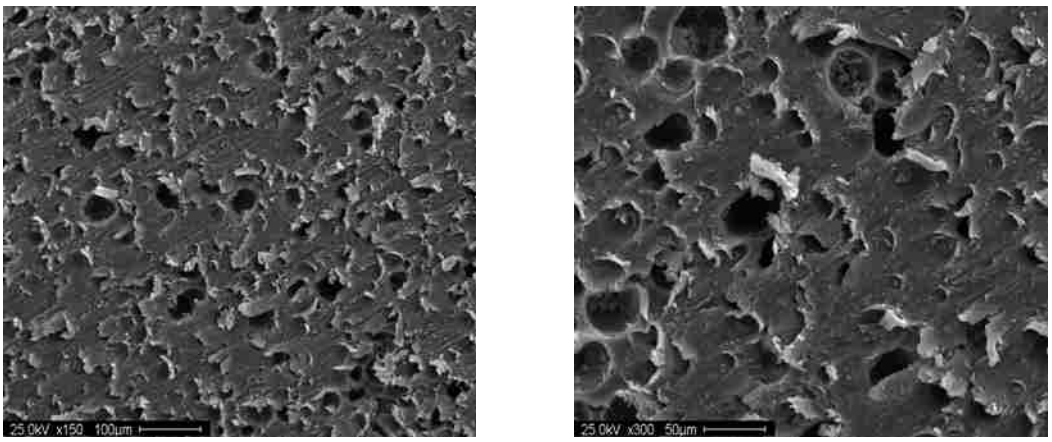

(a) (b)

Figure 2.22: SEM image of pad conditioned with 8µm abrasive for 20min at 150 rpm at two different magnifications (a)150X (b)300X

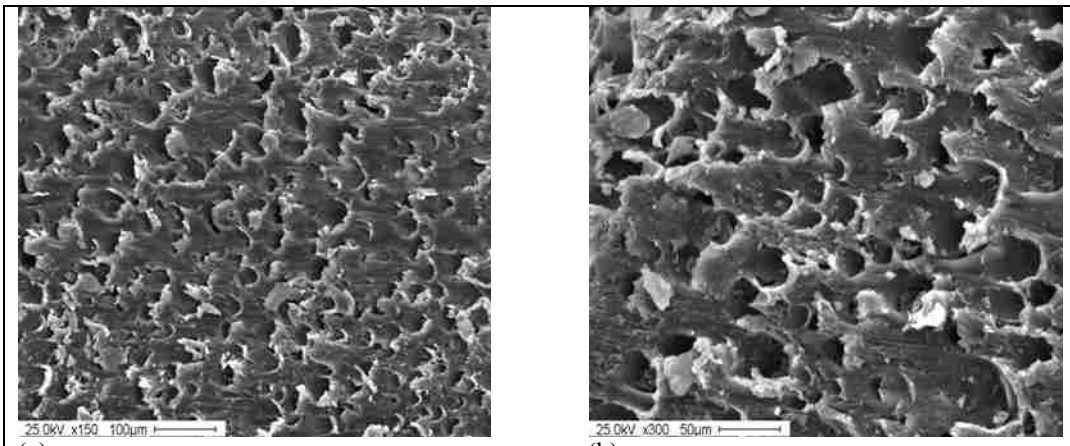

(a) (b)

Figure 2.23: SEM image of pad conditioned with 68µm abrasive for 20 min at 150 rpm at two different magnifications (a)150X (b)300X

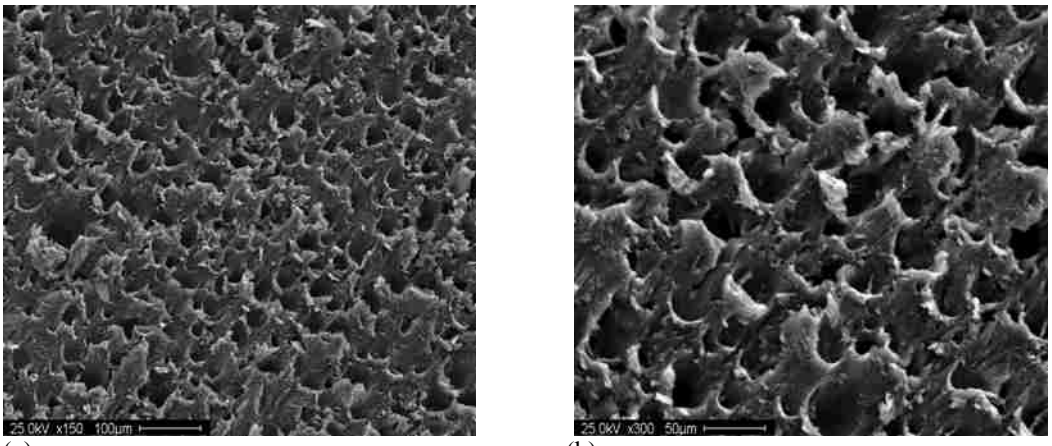

(a) (b)

Figure 2.24: SEM image of pad conditioned with 100µm abrasive for 20 min at 150 rpm at two different magnifications (a)150X (b)300X

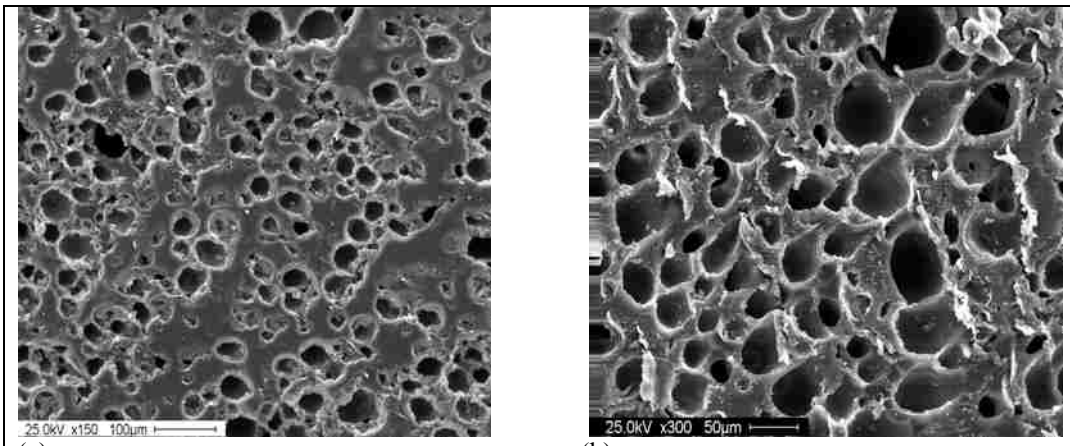

(a) (b)

Figure 2.25: SEM image of pad conditioned with 0.25µm abrasive for 5 min at 200 rpm at two different magnifications (a)150X (b)300X

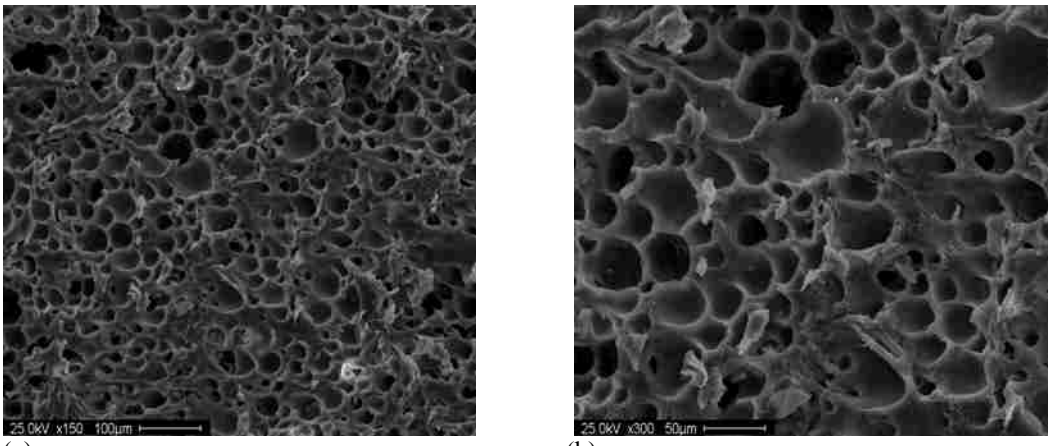

(a) (b)

Figure 2.26: SEM image of pad conditioned with 2µm abrasive for 5 min at 200 rpm at two different magnifications (a)150X (b)300X

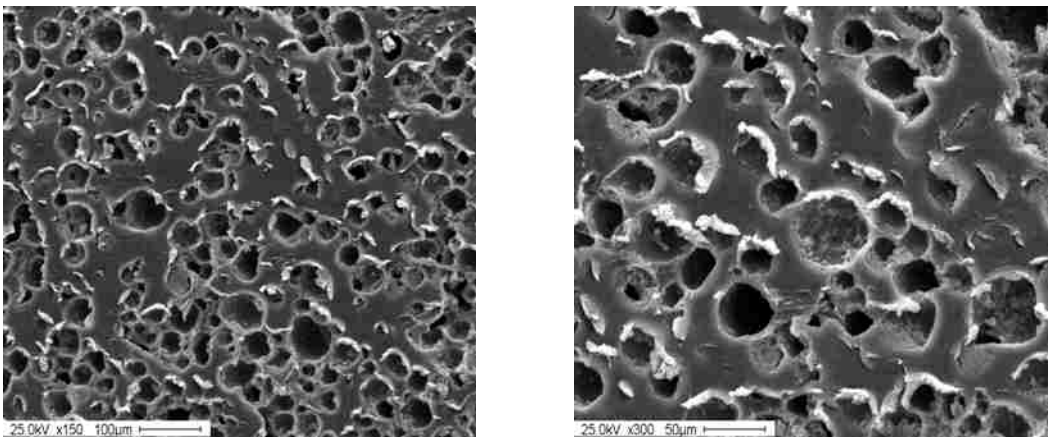

(a) (b)

Figure 2.27: SEM image of pad conditioned with 8µm abrasive for 5 min at 200 rpm at two different magnifications (a)150X (b)300X

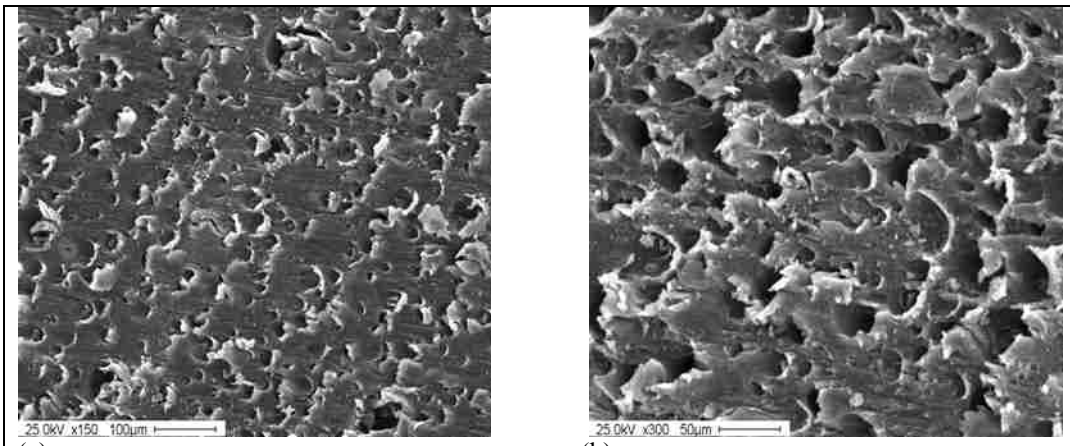

(a) (b)

Figure 2.28: SEM image of pad conditioned with 68µm abrasive for 5 min at 200 rpm at two different magnifications (a)150X (b)300X

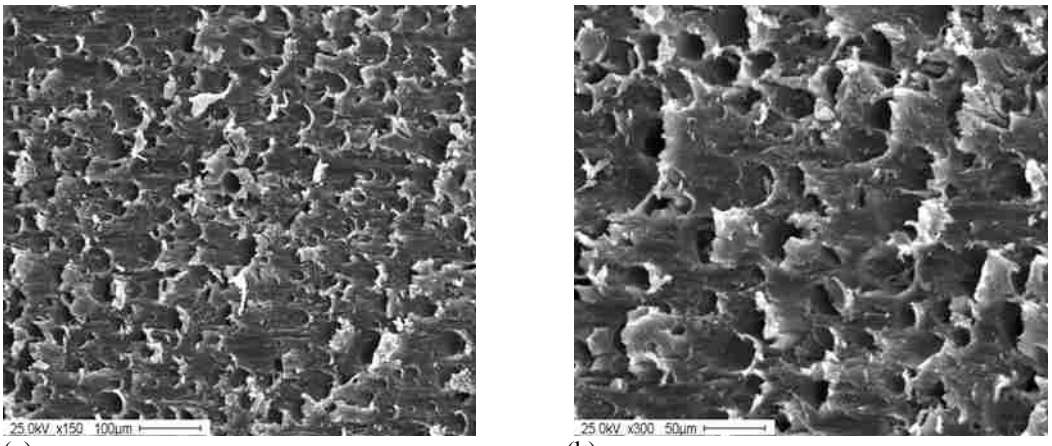

(a) (b)

Figure 2.29: SEM image of pad conditioned with 100µm abrasive for 5 min at 200 rpm at two different magnifications (a)150X (b)300X

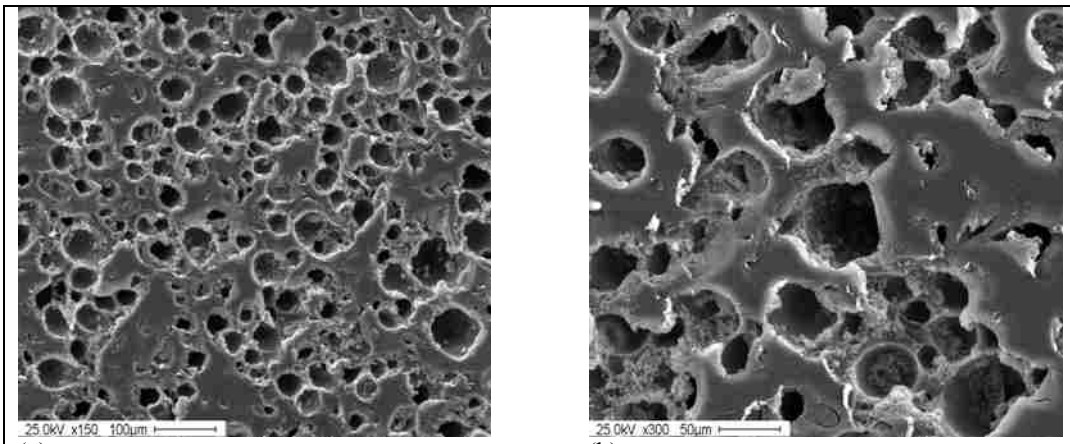

(a) (b)

Figure 2.30: SEM image of pad conditioned with 0.25µm abrasive for 20 min at 200 rpm at two different magnifications (a)150X (b)300X

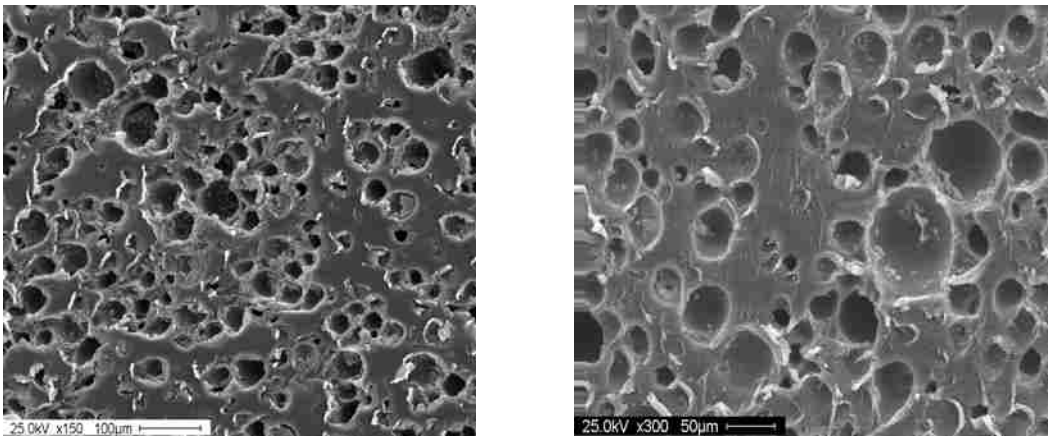

(a) (b)

Figure 2.31: SEM image of pad conditioned with 2µm abrasive for 20 min at 200 rpm at two different magnifications (a)150X (b)300X

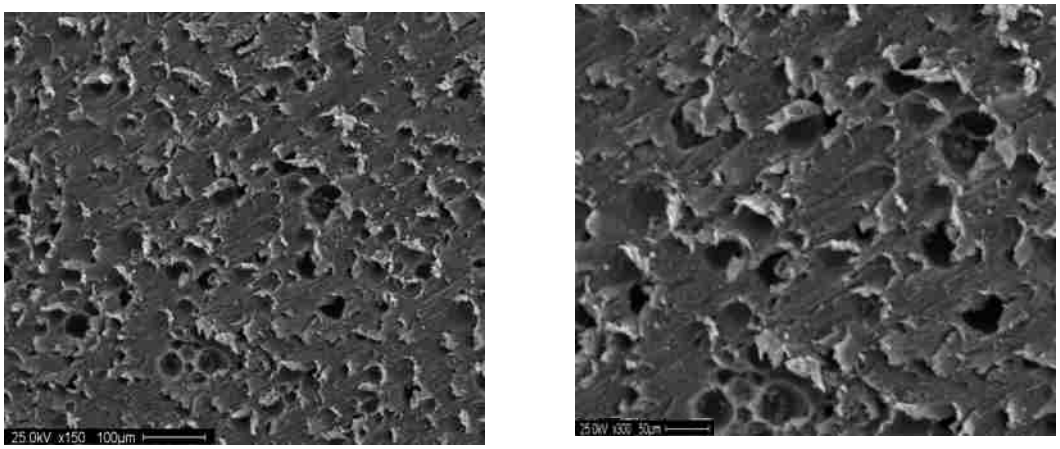

(a) (b)

Figure 2.32: SEM image of pad conditioned with 8µm abrasive for 20 min at 200 rpm at two different magnifications (a)150X (b)300X

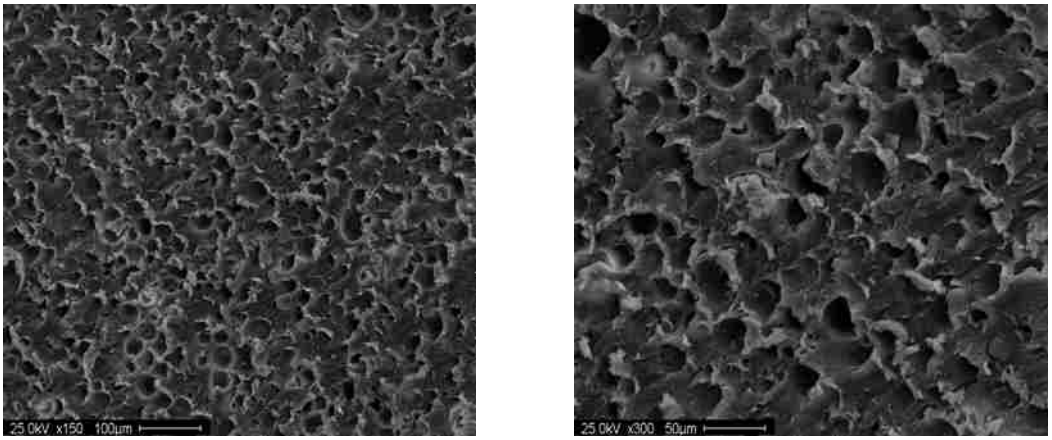

(a) (b)

Figure 2.33: SEM image of pad conditioned with 68µm abrasive for 20 min at 200 rpm at two different magnifications (a)150X (b)300X

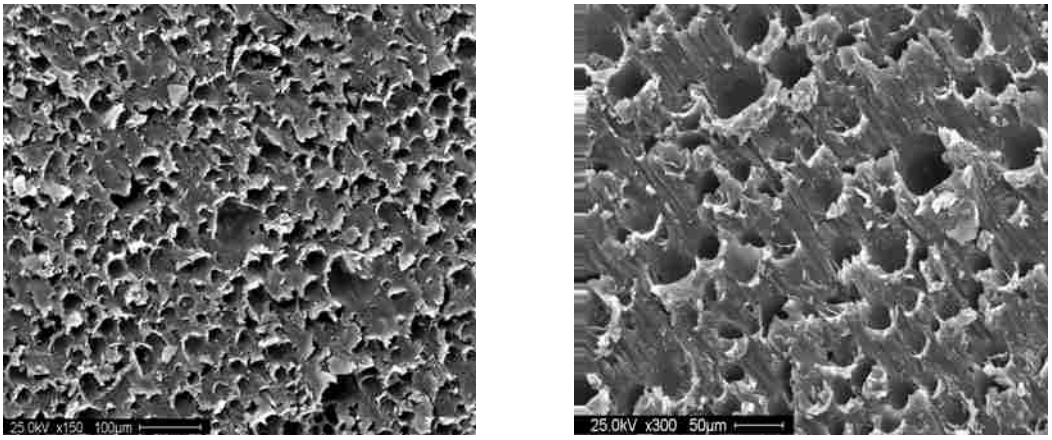

(a) (b)

Figure 2.34: SEM image of pad conditioned with 100µm abrasive for 20 min at 200 rpm at two different magnifications (a)150X (b)300X

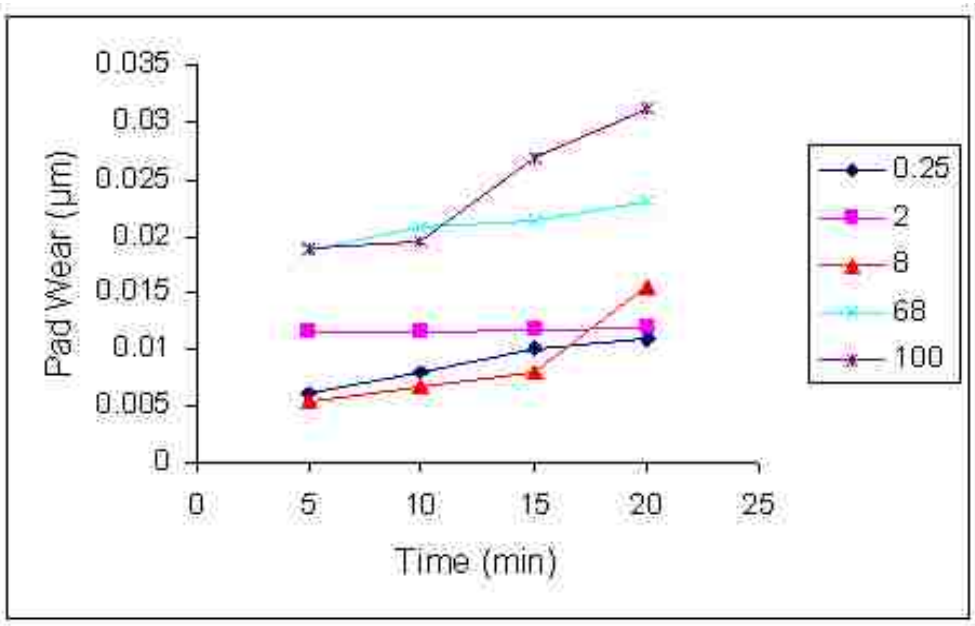

Figure 2.35: Plot of pad wear at different conditioning times for different abrasive sizes (µm) at 150 rpm

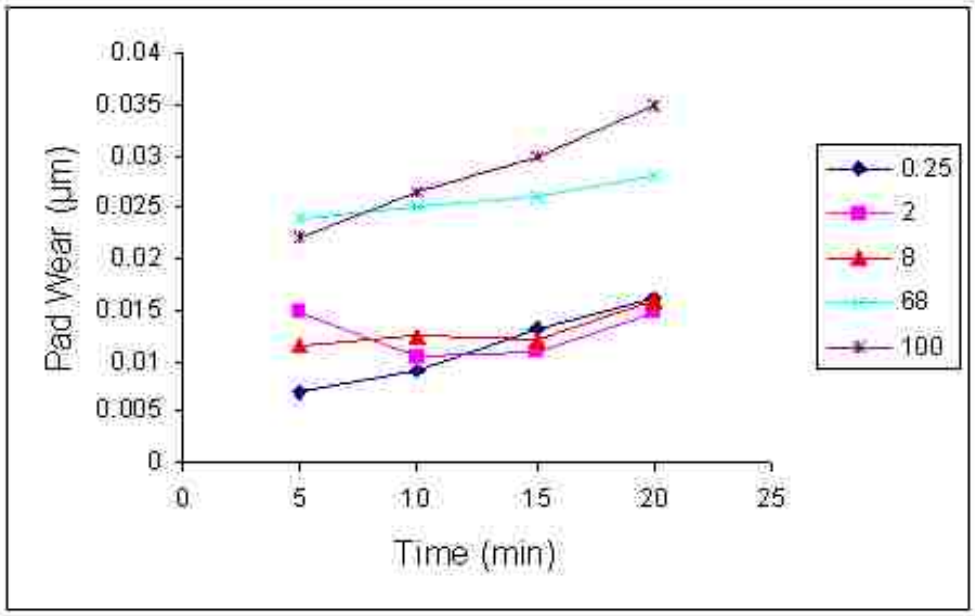

Figure 2.36: Plot of pad wear at different conditioning times for different abrasive sizes (µm) at 200 rpm

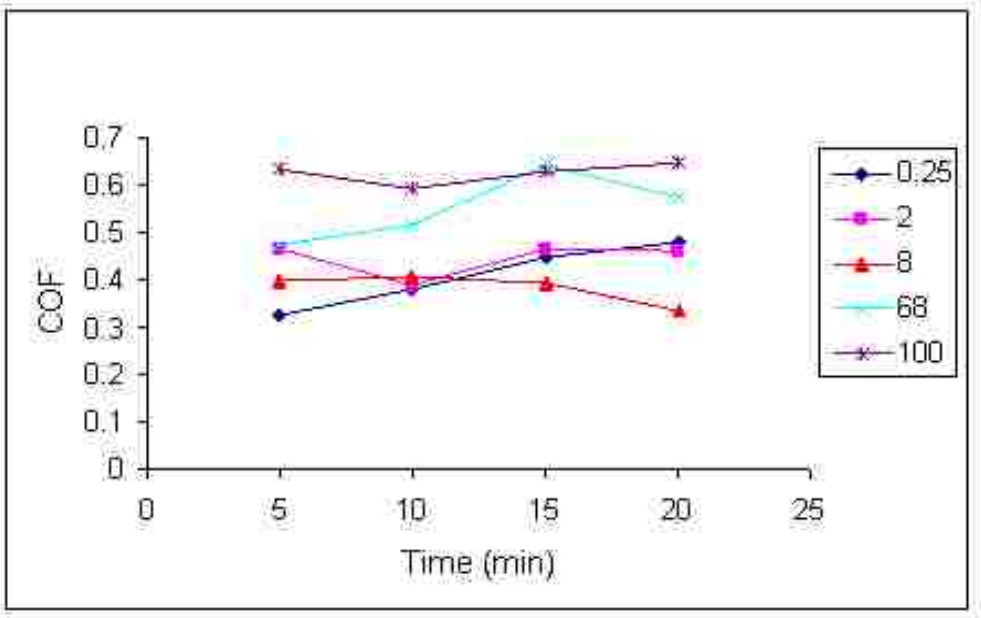

Figure 2.37: Plot of COF at different conditioning times for different abrasive sizes (μm) at 150 rpm

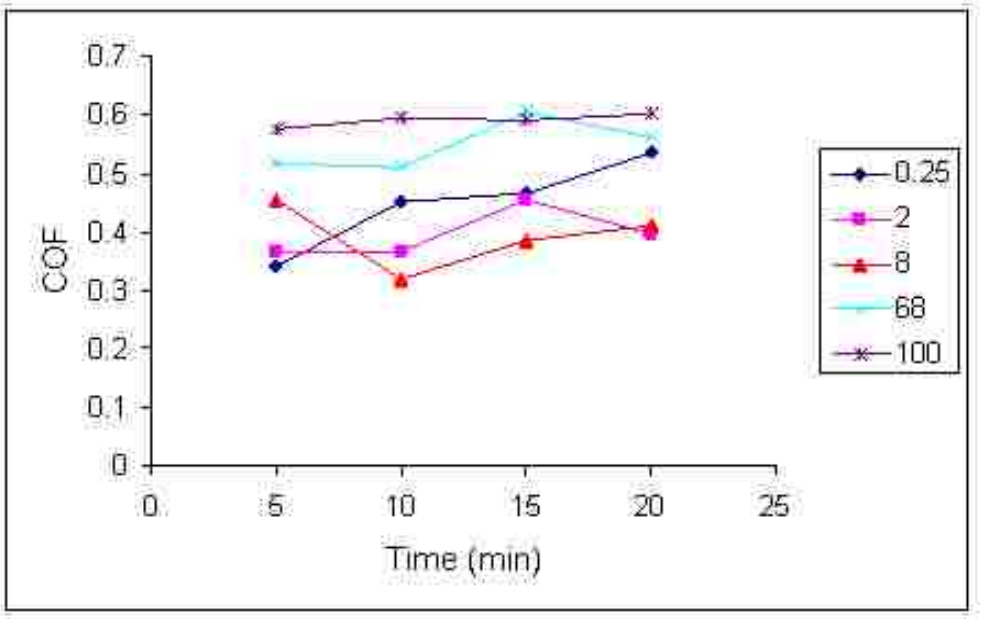

Figure 2.38: Plot of COF at different conditioning times for different abrasive sizes (μm) at 200 rpm

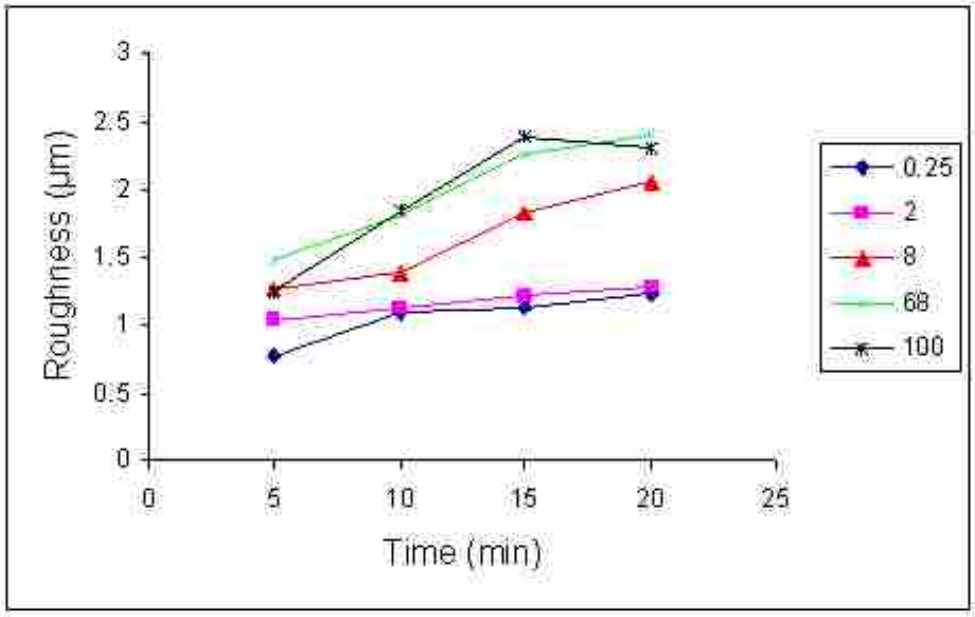

Figure 2.39: Plot of roughness at different conditioning times for different abrasive sizes (µm) at 150 rpm.

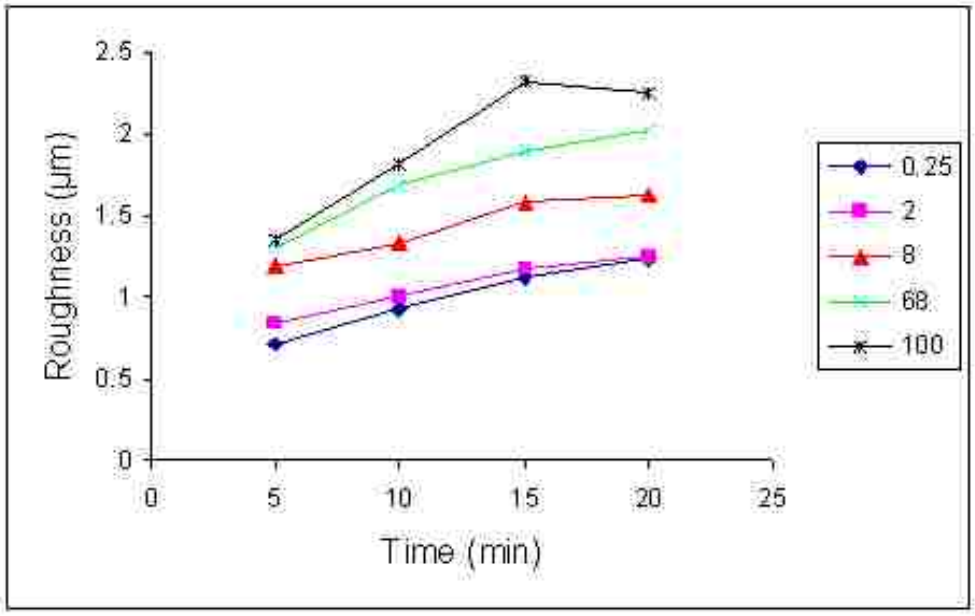

Figure 2.40: Plot of roughness at different conditioning times for different abrasive sizes (µm) at 200 rpm

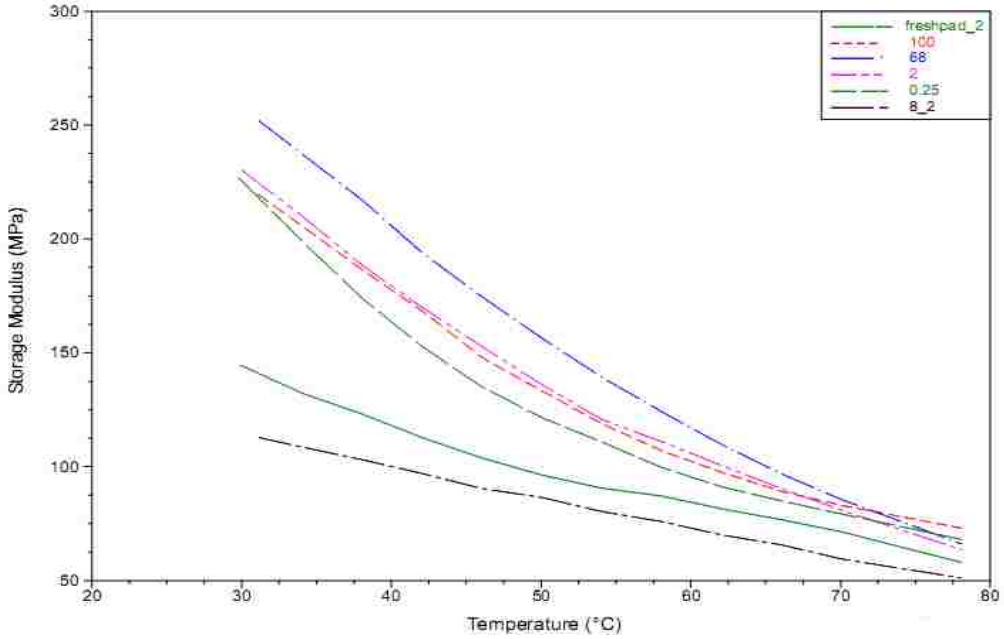

Figure 2.41: Plot of storage modulus at a frequency of 30 Hz for pads conditioned for 20 min with different abrasives

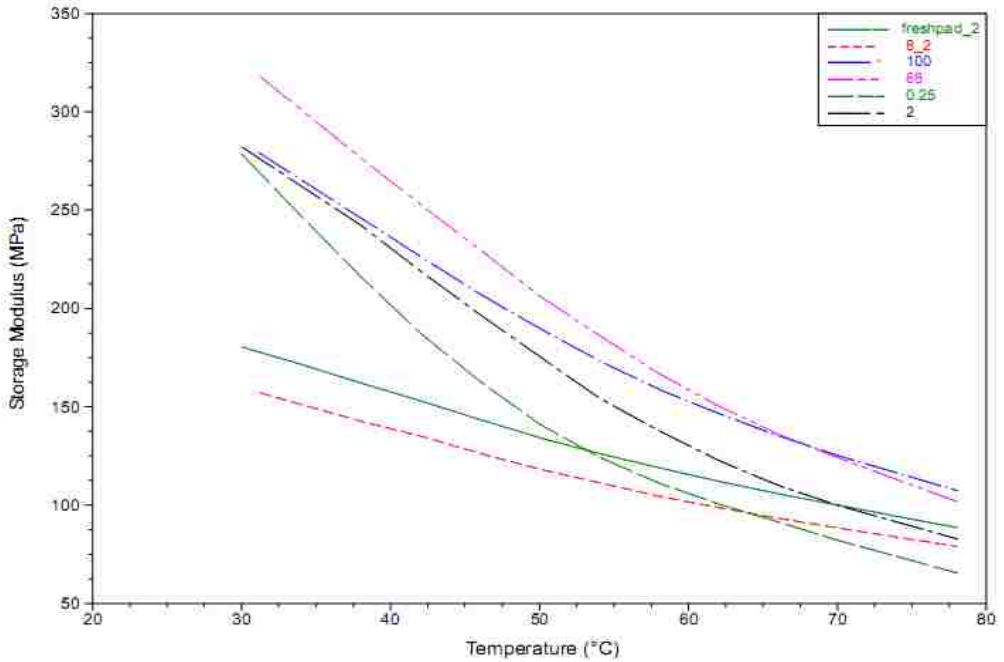

Figure 2.42: Plot of storage modulus at a frequency of 100Hz for pads conditioned for 20 min with different abrasives

Table 2.1: Experimental conditions for wafer polishing

Parameter	Value
Slurry flow rate	75 ml/min
Polishing Pad	Rodel IC 1000 SUBA IV
Wafer polished	2 inch blank copper wafers
Polishing time	3min
Platen speed	200 rpm

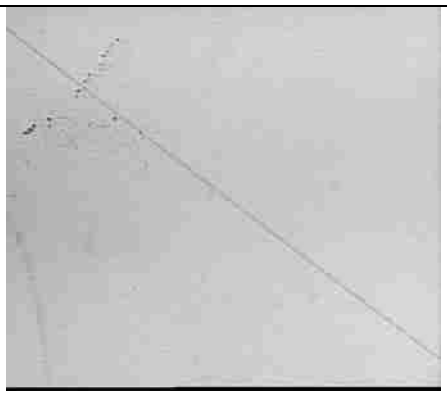

Figure 2.43: Optical image of first wafer polished on the pad conditioned with 8µm abrasive at 20X

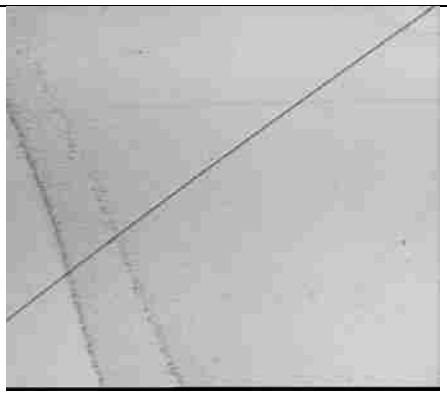

Figure 2.44: Optical image of third wafer polished on the pad conditioned with 8µm abrasive at 20X

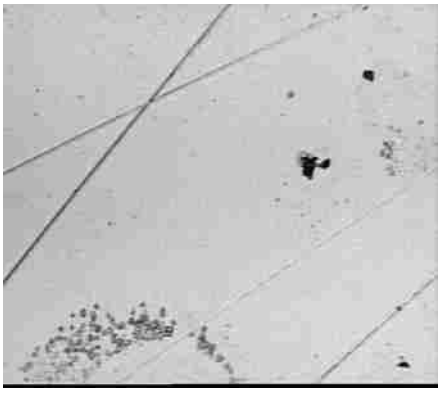

Figure 2.45: Optical image of first wafer polished on the pad conditioned with 68µm abrasive at 20X

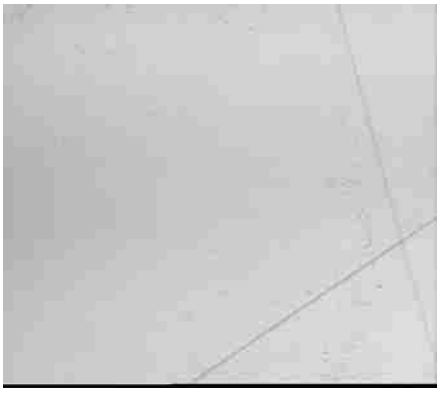

Figure 2.46: Optical image of third wafer polished on the pad conditioned with 68µm abrasive at 20X

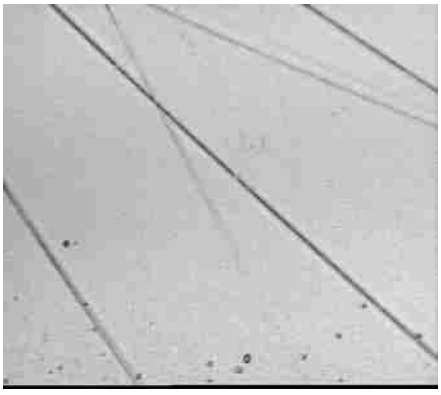

Figure 2.47: Optical image of first wafer polished on the pad conditioned with 100µm abrasive at 20X

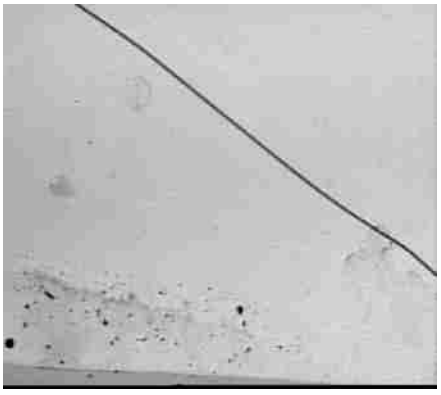

Figure 2.48: Optical image of third wafer polished on the pad conditioned with 100µm abrasive at 20X

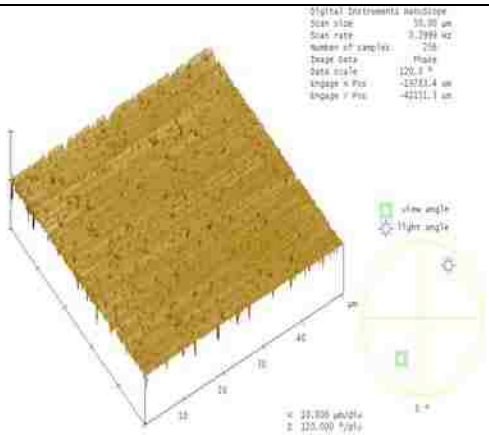

Figure 2.49: AFM image of the first wafer polished on a pad conditioned with 8µm abrasive

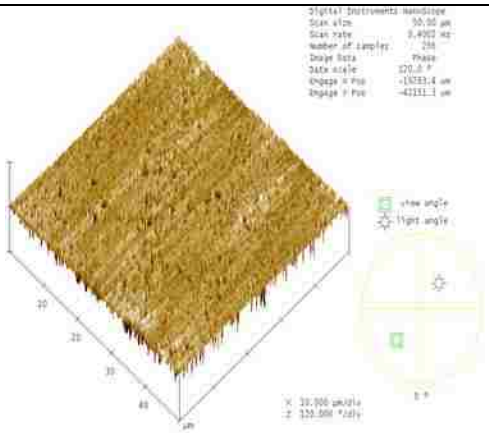

Figure 2.50: AFM image of the third wafer polished on a pad conditioned with 8µmabrasive

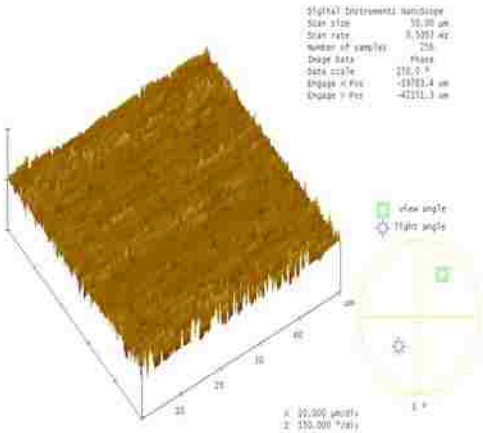

Figure 2.51: AFM image of the first wafer polished on a pad conditioned with 68µm abrasive

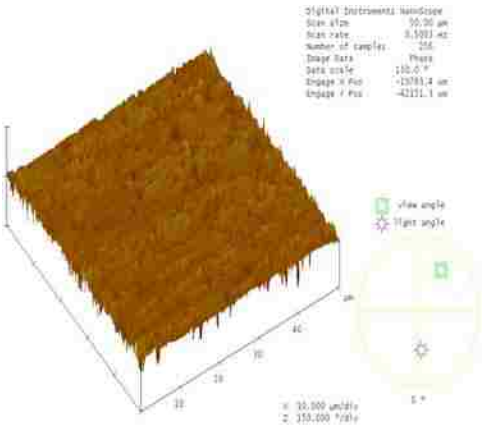

Figure 2.52: AFM image of the third wafer polished on a pad conditioned with 68µm abrasive

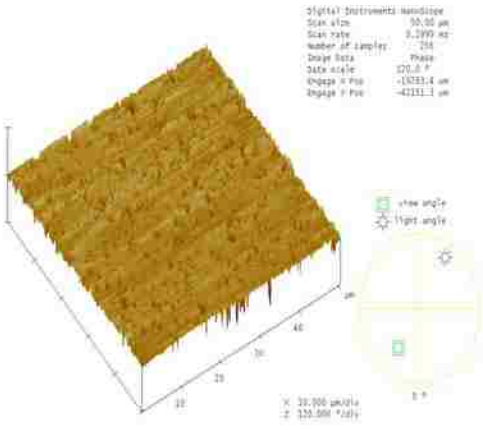

Figure 2.53: AFM image of the first wafer polished on a pad conditioned with 100µm abrasive

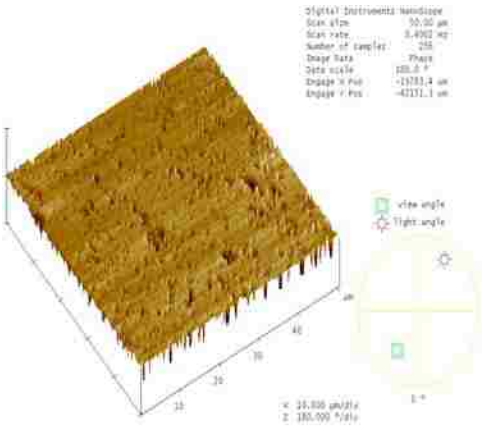

Figure 2.54: AFM image of the third wafer polished on a pad conditioned with 100µm abrasive

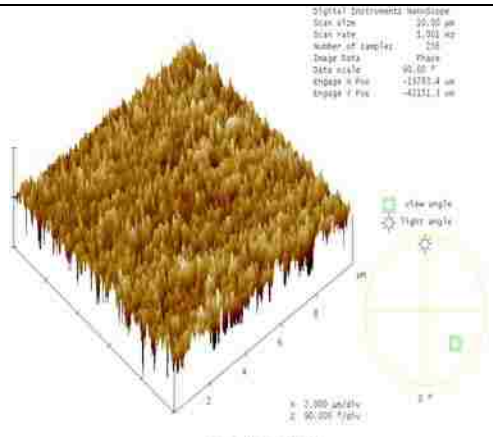

Figure 2.55: AFM image of pad conditioned with 8µm abrasive

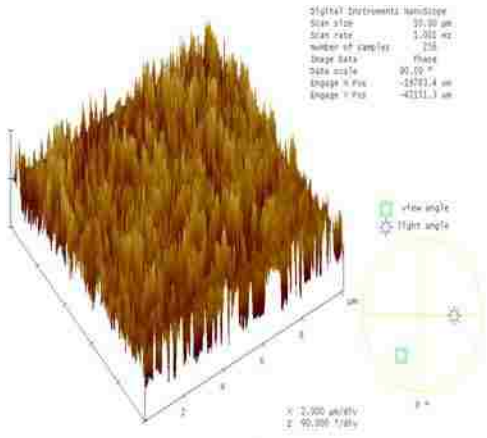

Figure 2.56: AFM image of pad conditioned with 68µm abrasive

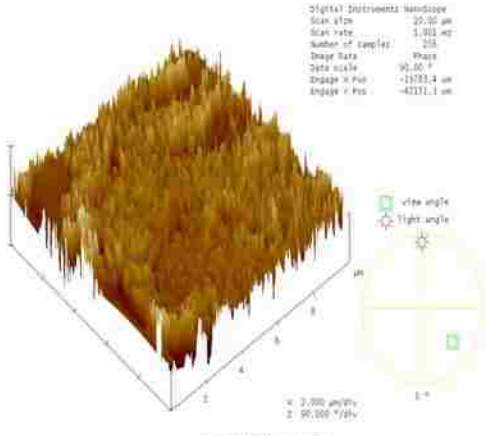

Figure 2.57: AFM image of pad conditioned with 100µm abrasive

Figure 2.58: SEM image of pad conditioned with 8µm abrasive

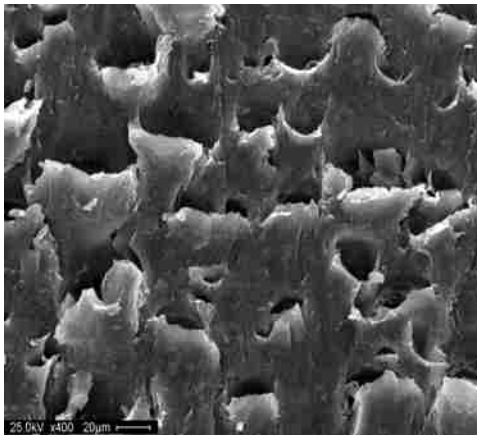

Figure 2.59: SEM image of pad conditioned with 68µm abrasive

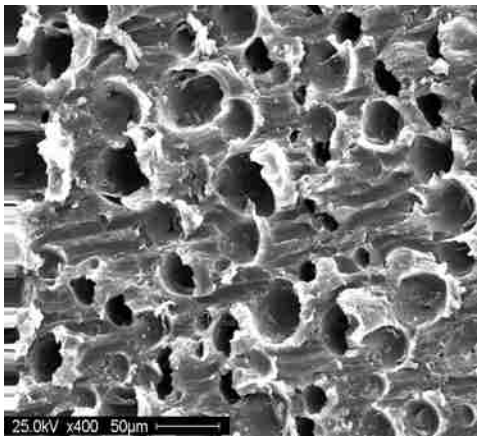

Figure 2.60: SEM image of pad conditioned with 100µm abrasive

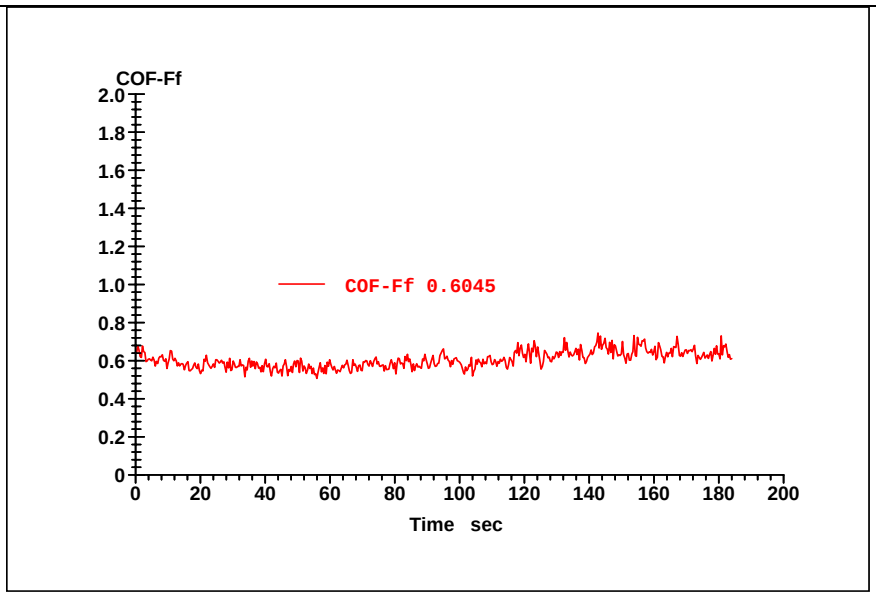

Figure 2.61: Plot of COF for abrasive size of 8µm

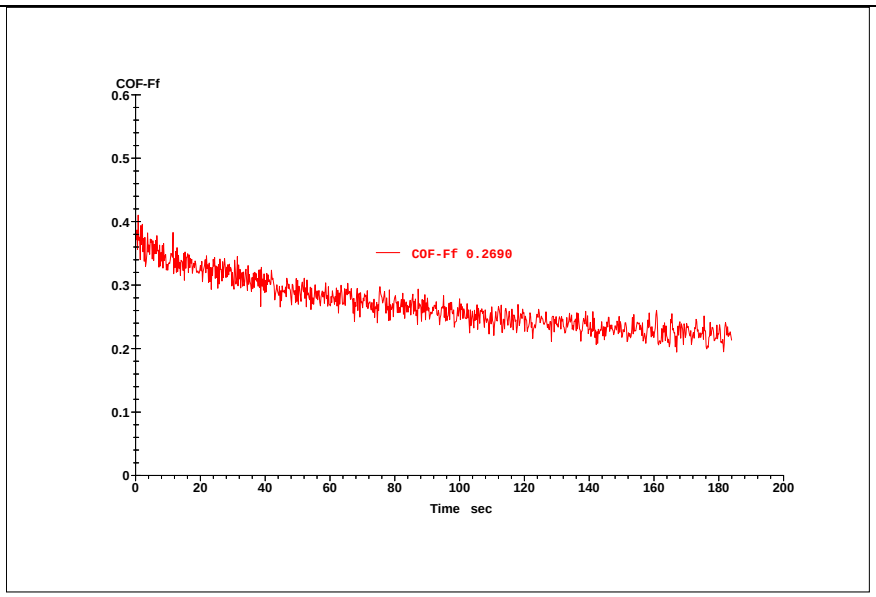

Figure 2.62: Plot of COF for abrasive size of 68µm

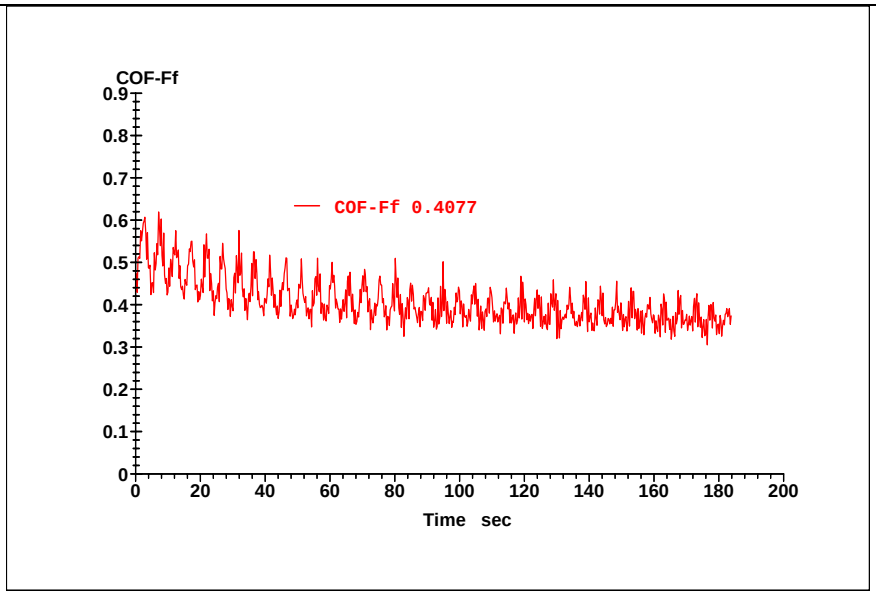

Figure 2.63: Plot of COF for abrasive size of 100µm

Chapter 3

Optical Measurement of the Contact Area between the Pad and Wafer

3.1. Concept of contact area and its importance

As described in chapter 2, the polishing pad is the platform on which the process of polishing is carried out. The wafer to be polished is held face down on the pad while the abrasive slurry flows between these 2 surfaces. As can be seen from Figure 3.1, the pad and the wafer come in contact at few points. The total area under these points of contact is known as the contact area. Since the pad is a polymer material, it does not have a very smooth or planar structure (Figure 3.1). The micro-hills and valleys on the pad material determine the contact area between the pad and the wafer. Some of the other factors affecting the contact area include down pressure, slurry-particle size, and wafer-pad rotating speed (*34*). The wafer-pad-slurry interactions can be understood better on the basis of micro- and nano-scale effects. At the micro-scale, particle based slurries interact with the pad and the wafer. The active particles in the slurry, trapped between the wafer surface and the pad cause the removal of material. At the nano-scale, the formation of a surface layer by the slurry chemicals and its removal as a result of abrasion, leads to the polishing effect(*35*)

Various techniques have been developed literature for measuring the roughness of the pad. For example, the Greenwood-Williamson elastic model (*36*) has been used to measure the roughness of the pad. This model is based on two assumptions. First, it is assumed that asperities have spherical shape. Second, it is assumed that the height and radius of asperities follow a Gaussian distribution.

It was found that the total area can be computed using the equation shown below.

$$A = \eta \int_{d}^{\infty} \int_{0}^{\infty} a \Phi_{\beta} \Phi_{z} d\beta dz$$

where, η is the density of the asperities; z is the height of the asperities; β is the radius of the asperities; Φ_{β} and Φ_{z} are Gaussian distribution functions.

The use of Fourier Transform Infrared Spectroscopy / Attenuated Total internal Reflection spectroscopy (FTIR/ATR) for the measurement of contact area has been explored in literature (*37*). In this technique, the area under the peaks of the spectra is measured to evaluate the intensities of the peaks. The intensity values were then compared with the intensities resulting from a 100% pad contact. A 100% pad contact implies that the pad used is non-porous, defect free and has a flat surface. This helps in determining the percentage of area contact. The results obtained using this technique were found to be similar to the results calculated by using the Greenwood-Elastic Model.

Figure 3.2 shows a plot of %contact area of the pad against applied load. The down pressure on the pad is evaluated by dividing the load applied to the wafer by the area of the wafer. The results obtained were found to be in agreement with the results obtained from the calculated results of Yu et al. From the graph it can be inferred that the contact area of the pad increases as the down pressure experienced by the wafer

increases. It may be inferred that as the down pressure increases, the area of contact increases which results in a higher degree of polishing of the wafer.

Evaluating the total area of contact between the pad and the wafer can give valuable information about the polishing run. The contact area information can be used to draw inferences about the effectiveness of the conditioning process. Amongst other factors, contact area depends upon the pad morphology or structure resulting from the process of conditioning. As was seen in Chapter 2, diamond abrasive size affects the pad morphology. Hence it can be inferred that, the diamond size on the conditioner affects the contact area between the pad and the wafer during polishing.

In order to evaluate the contact area, it is necessary to evaluate the 3D topography of the pad. Profilometry and laser interferometry are two techniques that can be used for evaluating the 3D topography of the pad. Though profilometry gives great images, it is limited by the fact that is a contact type method. On the other hand, interferometry, an optical technique requires the pad to be reflective in nature for measurement of the contact area, which again limits the use of this technique for the measurement purpose. Different factors affecting the contact area between the pad and the wafer have been investigated in literature. For example, confocal reflectance interference contrast microscopy (C-RICM) was used to evaluate the contact area (*38*). This technique uses light interference to recognize and measure the contact areas. A sapphire cover slip was used on a hard pad and then a soft pad made of porous polyurethane pad material. It was concluded that the contact area increases with the increase in the applied load. It was further observed that the conditioner type also affected the contact area and that different pads respond differently to conditioning. This is an ex-situ measurement.

Dual Emission Laser Induced Fluorescence (DELIF) has been used to study the interactions between the pad and the wafer (*39*). It can also be used to measure the in-situ thickness of the slurry. DELIF has been used in the past to study the pad wafer interaction in terms of average fluid layer thickness, compressibility of the asperity layer on the pad and measurement of surface roughness (*40*). This technique is based on the fluid layer profile formed at the interface of the pad and the wafer. At the contact points of the pad and wafer, the slurry thickness is zero. DELIF uses this principle to determine the area of contact. The percentage of contact area found using the DELIF method has been found to be in agreement with that found using the C-RICM method discussed above.

3.2. Measurement of contact area

This part of the thesis focuses on developing a simple method of measuring the contact area in contrast to the various techniques discussed above. The advantage of developing such a technique is that the process can be understood better and faster in order to observe the changes in the contact area as the polishing process progresses. The information that is obtained as a result of evaluating the contact area between the pad and the wafer provides a motivation for the research here. As part of this research the contact area is measured at different pressures while comparing the change in contact area due to changes in the applied pressures.

3.3. Experimental details

The preliminary research involved looking at the pad morphology under the optical microscope. The pad used for this experiment was IC 1000 which was conditioned earlier using a diamond conditioner.

The experimental setup, as shown in Figure 3.3, consisted of a pressure cell. The cell consisted of a circular disc with a cylindrical blind hole at the center. A cylindrical spacer was placed in the hole such that the top face of the spacer was flush with the top surface of the cylindrical disc. A small rectangular piece of the IC 1000 pad was cut and placed on top of the spacer. The size of the pad was such that it was smaller than the top surface of the cylinder. The pad was then covered by a cover slide. The cover slide acts as the wafer being polished.

The idea behind building this apparatus was to simulate the down pressure experienced by the wafer in a CMP process and observing the changes in the contact area of the pad. The operating principle of the apparatus is that as the vacuum between the cover slide and the spacer increases, the down pressure experienced by the cover slide increases. As the vacuum present in the space between the cover slide and the spacer was varied using a vacuum gauge, changes were observed in the contact area of the pad.

To begin with, a dry pad was placed on top of the spacer and was covered with the cover slide. The dry pad was observed under the optical microscope to evaluate its morphology. However, the pad morphology was not visible under dry conditions. Since real-time measurements involve the use of a wet pad, the dry pad was made wet using water and examined under the optical microscope. In order to clearly see the pad structure, a drop of pigmentation was added on the pad surface. This was done using a

commercially available blue ink. Once the wet pad surface was clearly seen, a laser was used to view the contact points. Laser sources of different power were used to get the best results. The laser was focused on the cover slide at an angle such that on hitting the cover slide over the pad, the laser beam undergoes total internal reflection. Due to internal reflection, several bright laser points were seen on the pad when it was observed under the optical microscope. Optical images were taken for dry and wet pads at different pressures and analyzed using software called ImagePro developed by MediaCybernetics.

3.4. Results and discussion

The optical microscope used for the study was a Nikon Measurescope UM-2 Tester. This microscope, shown in Figure 3.4, operates in reflected as well as transmitted light. It also operates in both, dark and bright field imaging modes. The contact area research was carried out in dark field in order to obtain clear images.

Figure 3.5 shows the optical images of the dry pad whereas Figure 3.6 shows the optical images of the wet pad. The images are captured at a magnification of 50X. As can be seen from Figure 3.5, it was difficult to observe the pad morphology when the dry pad was observed under the optical microscope. Before introducing the blue ink on the pad, the morphology could not be clearly observed for even for the wet pad as in Figure 3.6. It is not possible to evaluate the configuration of the pad surface though the pad surface can be seen in both the images. From these images, it is not possible to derive concrete inferences about the pad micro-structure, which is an important factor in determining the contact area. With the introduction of pigmentation (blue ink), the pad surface became much clearer as seen in Figure 3.7. Various hills and depressions can be observed from Figure 3.7 which is not clearly seen in Figure 3.5 and Figure 3.6. The conditioning trail

marks can be distinctly observed in Figure 3.7. Though an optical image does not deliver as much information as a SEM image (Figure 3.8), the optical method is a simpler technique to understand the pad microstructure.

Having observed the pad structure under the optical microscope, determining the contact area was the next step. When the laser beam was focused on the cover slide, certain bright spots could be seen under the microscope as seen in Figure 3.9. On observing closely, some of the bright spots showed debris deposited on the pad surface. This is evident from Figure 3.10. Figure 3.11 shows the surface of the pad while Figure 3.12 shows the optical image of the same spot on the pad as in Figure 3.11 but in presence of the laser beam. The laser was most effective in absence of the reflected light as it minimized the interference. Hence, all measurements were taken in the absence of reflected light. As discussed above, the pad-wafer contact area increases with an increase in down pressure. The same trend was followed by the observed laser points. On varying the vacuum and thereby varying the down pressure, the number of bright points also varied. With an increase in the down pressure, the number of bright points increased and with a decrease in the down pressure, the number of bright points decreased. This may be observed from Figure 3.13, Figure 3.14 and Figure 3.15. Apart from an increase in the number of points, the intensity of the points also increased. The change in the number and intensity of the laser points was used for the image analysis.

The software used for purposes of analysis was ImagePro. Analysis was first carried out on a dry pad and later on a wet pad using the laser and in absence of reflected light. For the analysis, the first optical image was taken at a magnification of 20X on a dry pad at a low pressure (Figure 3.16). The second image was taken at a higher pressure

(Figure 3.17) and at the same magnification. The number of points in Figure 3.16 is less than the number of points in Figure 3.17. Also, on comparison of the two images, the variation in intensity of the bright spots can be observed. Further, these optical images were analyzed using ImagePro to infer the change in the contact area resulting due to a change in down pressure. The analyzed image is shown in Figure 3.18. The change in intensity of a bright spot due to change in pressure can be observed in the analyzed image. For example, Figure 3.16 shows a point X. Figure 3.17 which is taken at a higher pressure contains the same point X but has a higher intensity. Figure 3.18 shows the image obtained by analyzing Figure 3.16 and Figure 3.17 using ImagePro. The point X can be observed in Figure 3.18 but the intensity of the point represents the difference in intensity as a result of the change in pressure. On an average, based on the analysis done at different points on the same pad surface and for three different pad samples, the resultant bright spots covered about 0.67% of the entire area, which represents the change in contact area with the change in pressure. For the dry pad, the average number of points seen on the surface was twenty five. Average statistics for the change in contact area are shown in Table 3.1.

Similar analysis was conducted for a wet pad. Figure 3.19 shows the image taken at lower pressure and Figure 3.20 shows the image taken at a higher pressure. The resulting difference due to change in pressure may be observed in Figure 3.21. In case of the wet pad, the bright spots cover about 0.85% of the entire area, which represents the change in contact area with the change in pressure on changing the pressure. Average statistics for the change in contact area are shown in Table 3.2.

Certain assumptions have been made during this analysis. The flaws in the cover slide have not been taken into consideration. The defects in the cover slide may reflect some light and cause some bright spots in the image. But, it was assumed that when the images are being subtracted, these bright spots tend to nullify. The other factor that has not been accounted for is the presence of debris which showed up as bright spots. Since the position of the debris does not change on changing the pressure, it may be assumed that it cancels on analyzing the images. However, the intensity of the bright spots representing the debris may change due to change in the down pressure. Therefore, on analyzing the images using ImagePro, the debris may show up as a bright spot in the analyzed image with a different intensity. Hence the debris may contribute towards the change in contact area. In other words, if debris is present, the actual change in contact area may be lesser than the calculated change.

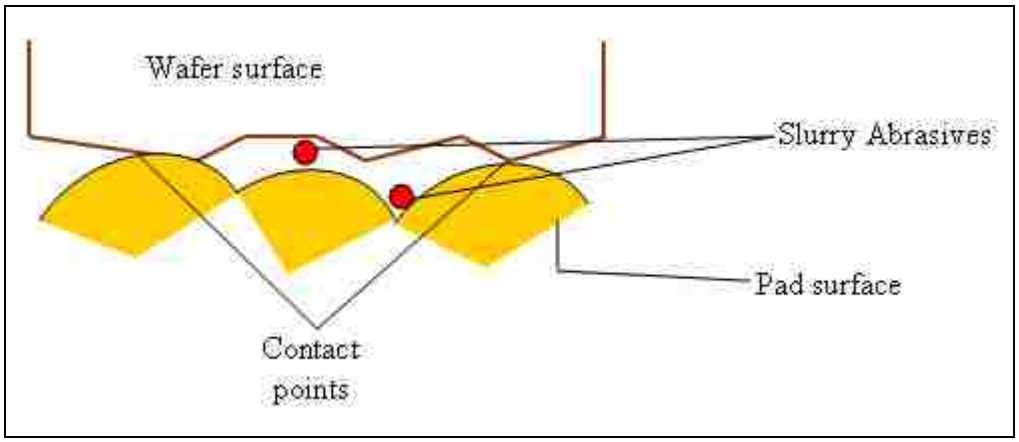

Figure 3.1: A schematic diagram depicting contact points between pad and wafer during polishing

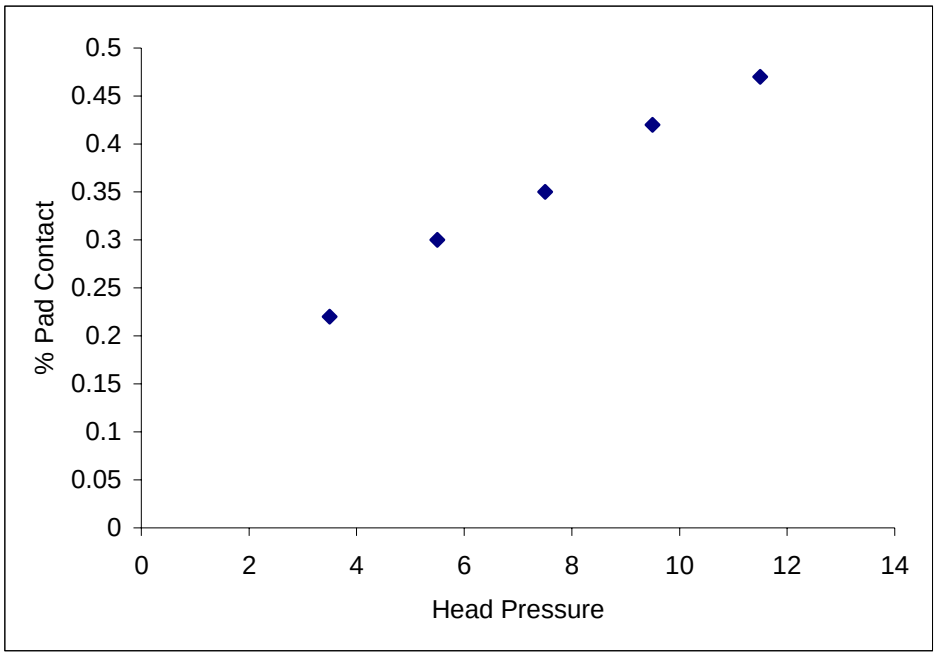

Figure 3.2: Plot of % pad contact vs. head pressure. The data in the figure is from the literature (*37*)

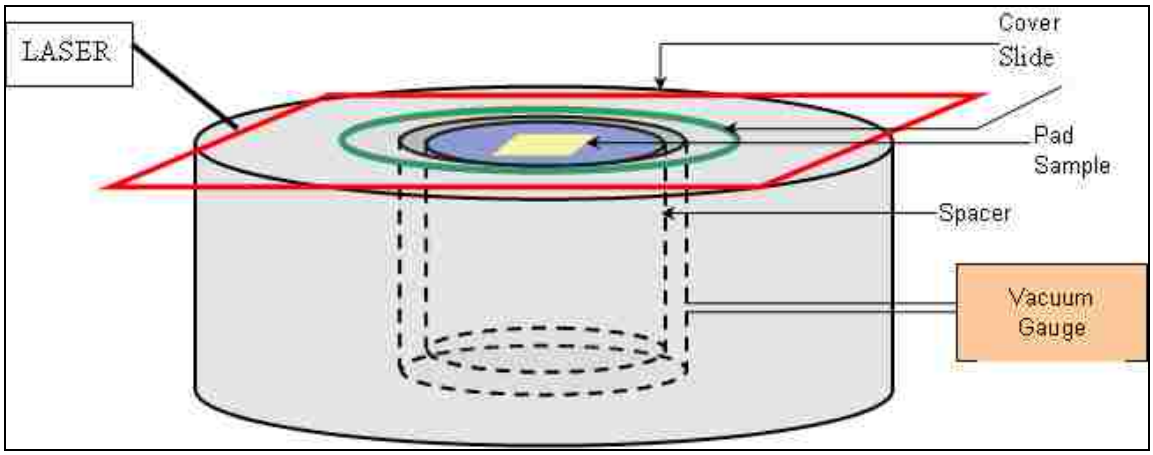

Figure 3.3: A schematic diagram of the experimental setup for measuring contact area

Figure 3.4: Nikon measurescope UM-2 tester

Figure 3.5: Optical image of dry pad at 20X

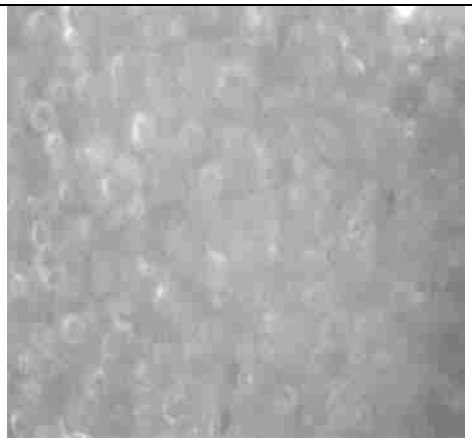

Figure 3.6: Optical image of wet pad at 20X

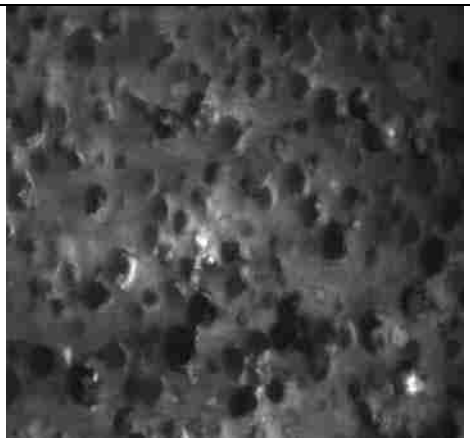

Figure 3.7: Optical image of wet pad after introduction of blue ink at 20X

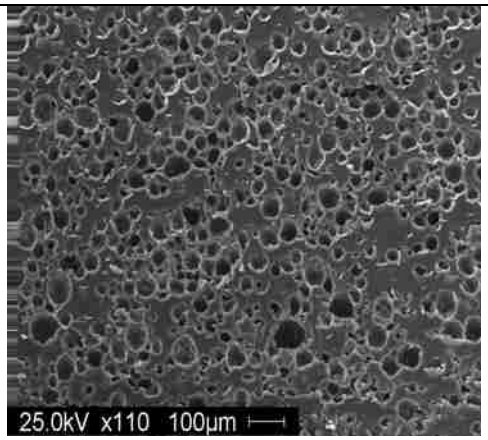

Figure 3.8: SEM image of a pad

Figure 3.9: Optical image of wet pad with a focused laser at 20X

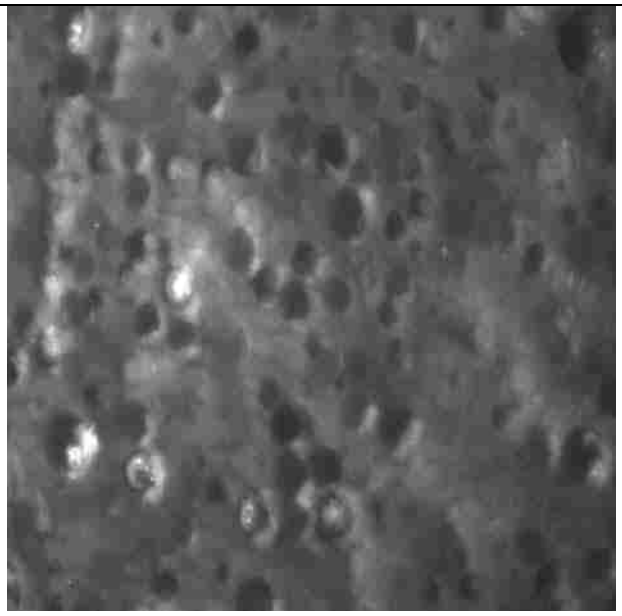

Figure 3.10: Optical image of a pad at 20X showing laser points that represent the debris on the pad

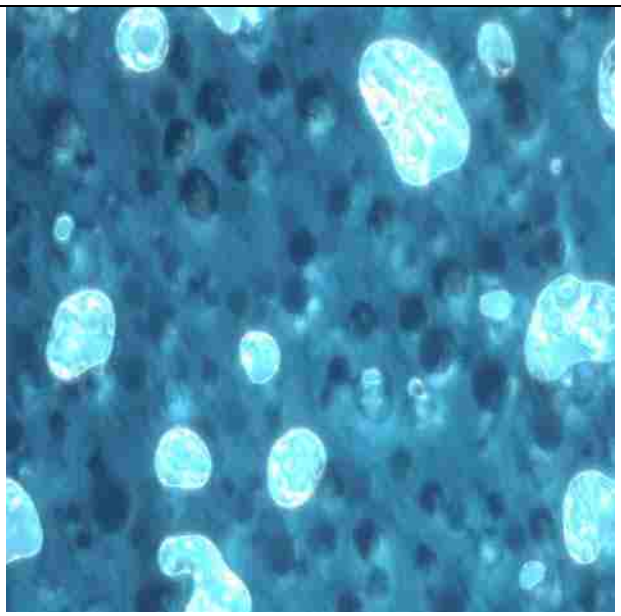

Figure 3.11: Optical image of wet pad at 20X

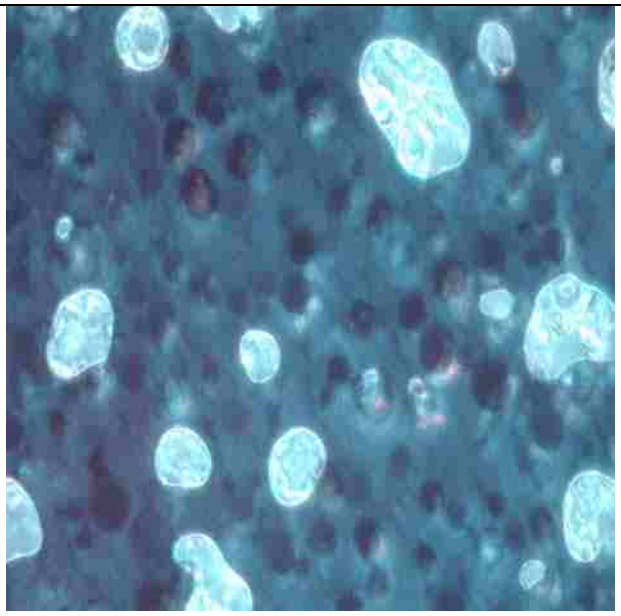

Figure 3.12: Optical image of wet pad with laser points at 20X

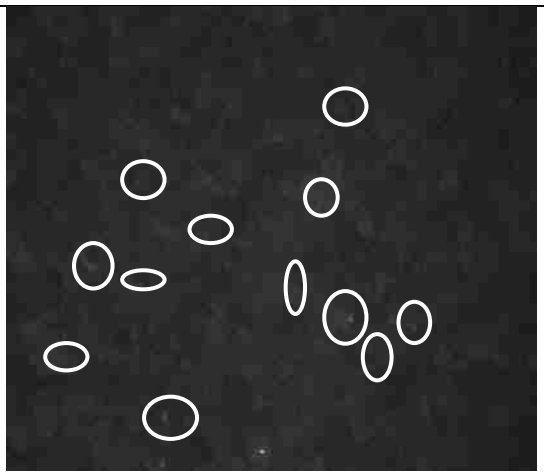

Figure 3.13: Optical image of pad at 30 torr

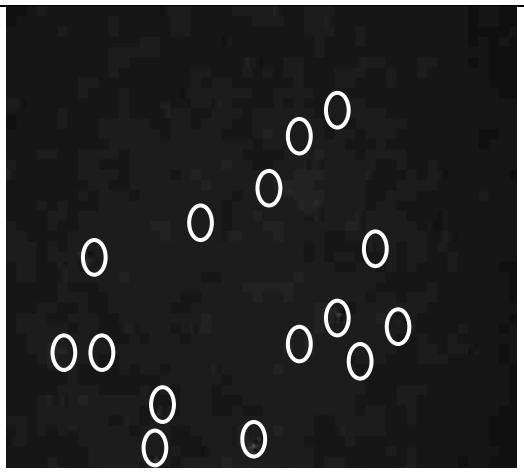

Figure 3.14: Optical image of pad at 50 torr

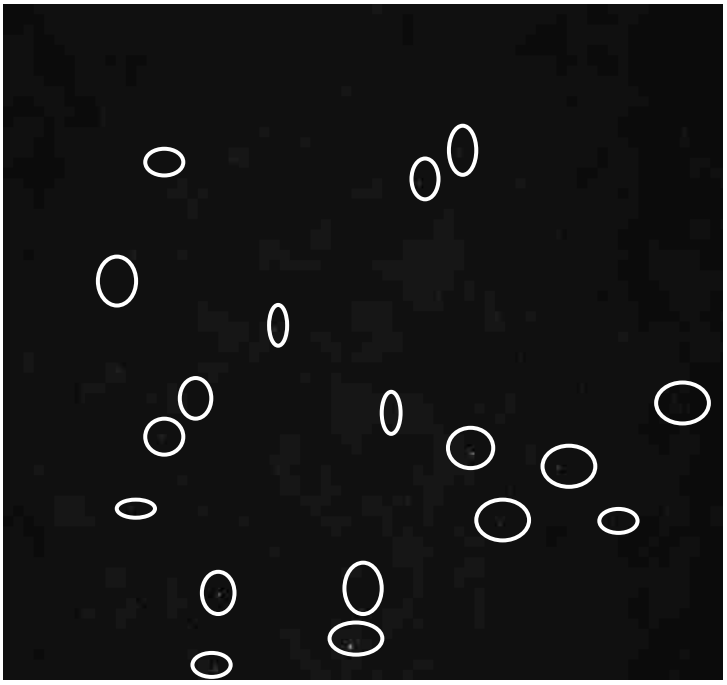

Figure 3.15: Optical image of pad at 70 torr

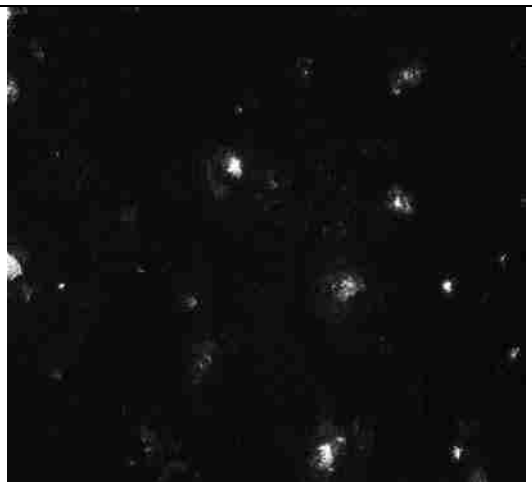

Figure 3.16: Optical image of pad showing contact points at 30 torr

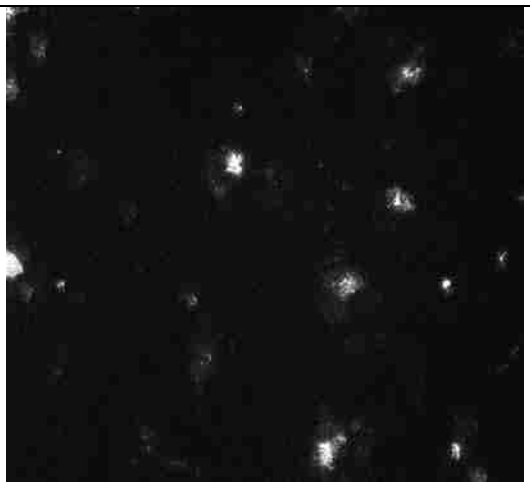

Figure 3.17: Optical image of pad showing contact points at 50 torr

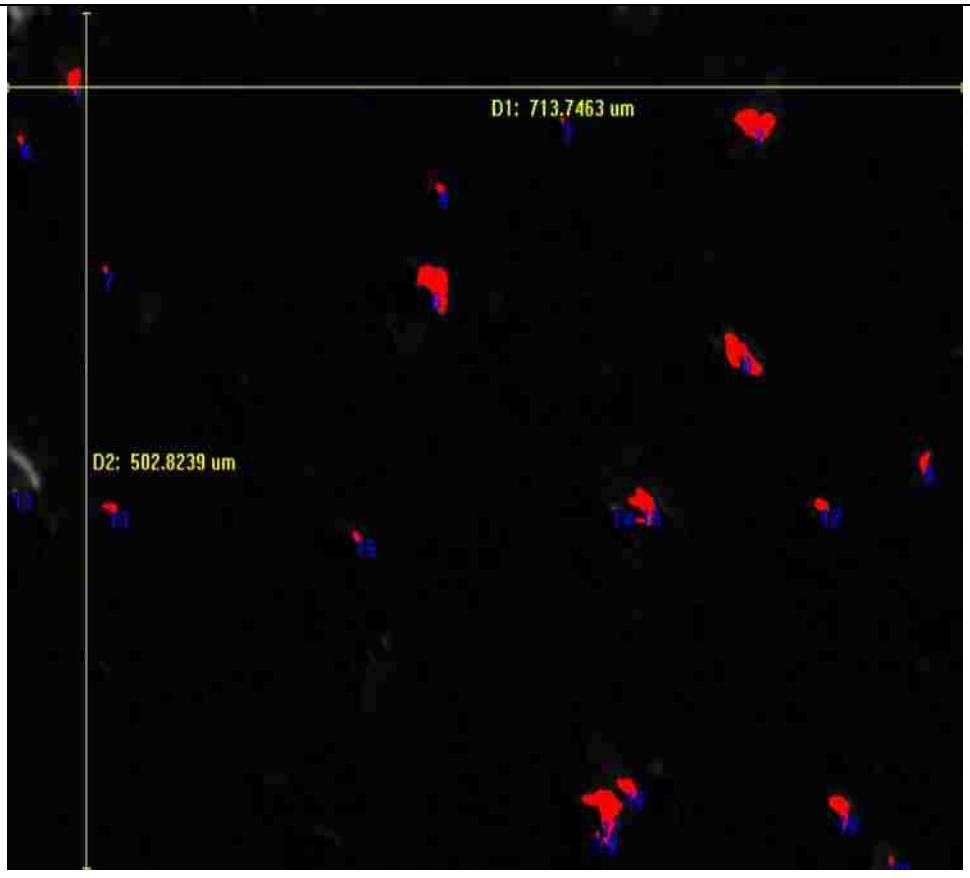

Figure 3.18: Image showing analysis performed by ImagePro

Figure 3.19: Optical image of wet pad at 30 torr

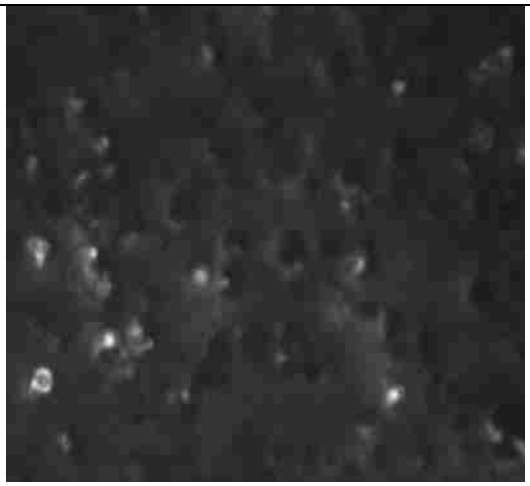

Figure 3.20: Optical image of wet pad at 50 torr

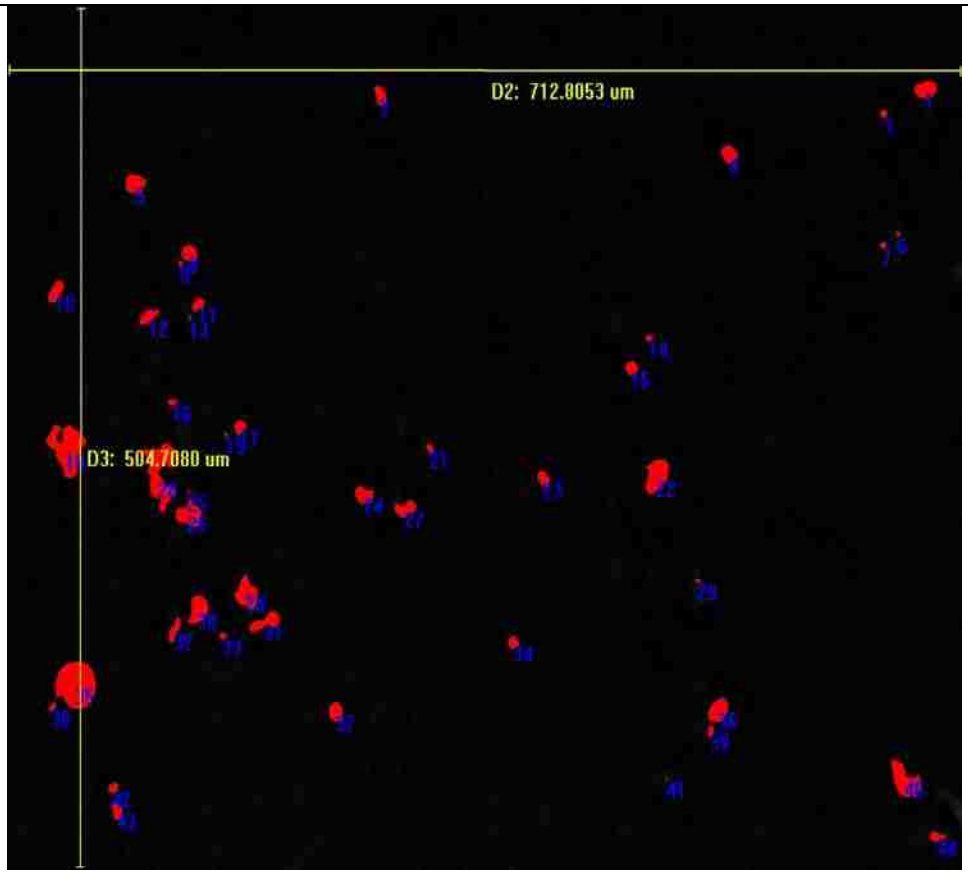

Figure 3.21: Image showing analysis performed by ImagePro

Table 3.1: Statistics showing the change in contact area for a dry pad

Stats	Area	Diameter (mean)
Min	3.77	2.23
Object Number	14	14
Max	408.74	22.07
Object Number	17	6
Range	404.97	19.84
Mean	121.02	10.05
Std.Dev	140.39	6.88
Sum	2420.53	201.04
Samples	20	20

Table 3.2: Statistics showing the change in contact area for a wet pad

Stats	Area	Diameter (mean)
Min	2.438	1.767
Object Number	25	25
Max	648.80	28.23
Object Number	35	35
Range	646.36	26.46
Mean	106.73	9.62
Std.Dev	139.67	6.31
Sum	3057.94	423.27
Samples	44	44

Chapter 4

Synthesis of Zirconia Nanoparticles through Plasma Route for CMP Slurry Applications

4.1. Synthesis of zirconia through various methods

Aerosol technology has been considered advantageous over the other methods for using small liquid volumes and for being less expensive for the nanoparticle synthesis (*41*). Hartmann et al.(*42*) used zirconium tetrachloride in oxygen flame to get fluffy tetragonal zirconia particles with diameters ranging from 10nm to 50nm. The properties of these particles were controlled by the flame temperature. Another technique known as flame spray pyrolysis, (FSP) which is a single step method and a low cost process, was used by Nielson et al. (*43*) to make 5μm zirconia particles. They used zirconium sulfate as the precursor. Karthikeyan et al. (*44*), following the FSP approach, used zirconium n-butoxide in butanol as a precursor, and synthesized tetragonal zirconia nanoparticles with diameters ranging from 12nm to 21nm. The same precursor, zirconium n-butoxide, was later used by Yuan et al.(*45*) to make micrometer and smaller sized powders. These methods and results were later verified by many groups that followed. It was seen that all the results obtained so far using FSP showed a dominant tetragonal phase and a minor

monoclinic phase. Further investigation showed that these studies did not emphasize on the various factors affecting the particle size.

Work carried out by Mueller et al (*41*) showed the importance of precursor concentration, flow rate of dispersant gas on the morphology, size distribution and crystallinity of the zirconia nanoparticles following the FSP method. They concluded that higher gas flow rate resulted in smaller flame heights, therefore, giving smaller particle size. Large aggregated particles were seen with high precursor concentrations which is in disagreement with the findings of Killian et al.(*46*). To explain the co-existence of the two phases, it was shown the fast quenching resulted in the tetragonal phase which decreased with the longer residence time and appearance of monoclinic structures. The earlier work, using reverse emulsion technique carried out by Kanai et al., and Ramamurthi et al.(*47*) was done by bubbling ammonia gas through zirconium (IV) ion giving a non-uniform particle size distribution of zirconia. This gave way to the two-emulsion technique. The technique involves the use of two reverse emulsions with metal containing aqueous solutions or aqueous ammonia that are suspended in oil. The size and shape of particles so produced is controlled by the size of the droplets, which can in turn be controlled using a surfactant. The two-emulsion precipitation technique was used by Tai et al.(*48*) for controlling the particle size of zirconia. They showed that the morphology and size distribution of particles was affected by the stability of the emulsion. The macro-emulsion, prepared using heptane for the oil phase, showed larger particle size, wider particle size distribution, and less agglomeration with a high solute concentration. For the micro-emulsion system that was prepared using cyclohexane, the size was seen to increase with an increase in the zirconia (IV) ion. Hu et al. (*49*) worked

on the synthesis of hydrous zirconia nanoparticles by forced hydrolysis. This method comprises of homogeneous hydrolysis and controlled polymerization of tetramers of zirconium and is performed in the aqueous solution of inorganic salts. The resulting powder was found to be porous monoclinic nanocrystalline zirconia with an average size of 5nm. Another paper by Srdic et al.(*50*) talks about chemical vapor synthesis of alumina doped nano zirconia. The average particle size was about 5 nm with 3 and 30% of surface alumina. They further concluded that the presence of alumina, even at very low concentrations, changed the properties of the zirconia. Zirconia powders have also been synthesized using the sol-gel process, i.e. by hydrolysis and condensation of alkoxides of zirconium. The powders formed at room temperature, by this process are amorphous in nature (*51*). Another technique used for synthesis is the low temperature combustion. The product is voluminous in nature. On characterization, nano-zirconia showed a compact distribution of particles with the size ≤ 20 nm (*52*). The inert gas condensation (IGC) technique employs pure metal or monoxide evaporation in presence of helium at low atmospheric conditions followed by post-deposition (*53-56*) oxidation. This process resulted in non-agglomerating zirconia nanopowders with a size distribution of 4-14 nm (*57*).

Though there are various methods for the production of nanopowders as described above, these have some limitations. Some of them display a wide particle size distribution while others show agglomeration problems. Post-treatment needed in some cases for the end product results in sintering problems. Cost and mass production is the limiting factor for many methods. To overcome these issues, the plasma route for the synthesis of nanoparticles has been of great interest (*58*).

4.2. Plasma synthesis of nanopowders

Nanopowders are now being synthesized using the plasma route because of advantages such as providing high temperatures zones, energy concentration, rapid quenching and above all, a clean environment.

In the plasma processing of nano-powders, thermal plasma with high energy is used to generate precursors in the vapor phase to synthesize nano-powders, when quenched. Synthesis of metals, ceramics, or composites has shown that thermal plasma route is one of the most promising methods for producing nano-powders. There are several stages in the plasma synthesis. These include, injection of the reactant in the plasma, reaction to form the product, quenching leading to the nucleation and growth of the particles (*59*). Parameters such as temperature, pressure, flow rate and power control the particle properties. The end powder can be characterized by small particle size, high purity and high activity (*60*). Some of the nanopowders synthesized via the plasma synthesis are discussed below:

1. Oxides: Alumina nanopowder is synthesized in a DC arc plasma under atmospheric conditions using Al electrodes (*61, 62*). These particles show a spherical shape. Titania nanopowder (*62*) which is again spherical in shape is made from the reaction between $TiCl_4$ and O_2. It is also prepared from TiC in the Ar-O_2 plasma (*63*). Other oxides prepared include CeO_2, Y_2O_3, ZrO_2 and Cr_2O_3.
2. Nitrides: Aluminium Nitride (AlN), is synthesized using an aluminium anode with an interaction between Al and N_2/NH_3(*64*). Silicon nitride (Si_3N_4) is prepared from the reaction between silicon powder and ammonia in an arc plasma

(*64*). The other nitrides that are prepared by the plasma route include TiN and Mg_3N_2 (*65-69*).

3. Carbides: Silicon Carbide is synthesized using Si and CH_4 in an induction plasma (*70, 71*).Tungsten Carbide is generally prepared using a dual RF plasma. The other carbides that are being successfully prepared include those of titanium and boron.

When carrying out the synthesis in gas phase, a balance has to be achieved in obtaining high production and faster rates and formation of agglomerates. The plasma route for synthesis helps in overcoming the issues of low temperatures and low reaction rates that are responsible for formation of chunks of nanoparticles. This is done by electrically charging the particles. One of the major limitation of the plasma route is collection of the end product is generally a very small amount (*72*).

4.3. Zirconia nanoparticles through the plasma route

Zirconia, crystalline oxide of the zirconium is categorized as the most promising ceramic materials of today. With a molar mass of 123.22g/mol and a density of 5.89 g/cm^3, this white crystalline solid finds use in many engineering applications.

Zirconia is in monoclinic phase at room temperature and is seen to change its phase to tetragonal at relatively higher temperatures. But small particles are seen to exhibit the tetragonal phase at room temperature as this is energetically favored while in the larger particles monoclinic phase is favored. The stresses caused due to the change in phase result in cracking of the ceramic on cooling. This calls for stabilization using different oxides. Some of the common oxides used for this purpose are magnesium oxide, calcium oxide, cerium oxide and yttrium oxide (*41*). Studies have shown that yttria

stabilized zirconia (YSZ) has a higher resistance to the low temperature effects compared to the YSZ prepared by conventional methods(*60*).

Vollath and Szabo described the synthesis of zirconia nanopowders by microwave plasma(*72*). Here, the operating temperature of the gas is lower than DC or RF plasma. The zirconia nanoparticles obtained by this route are about 5nm in size and are in the form of single crystals. Alumina coated zirconia nanoparticles synthesized using microwave plasma are crystalline in nature with a glassy coating. The size of zirconia can be controlled by varying the production rates, concentration of precursor, and flow rate of gas dispersion(*41*).

Ultra-fine powders of yttria stabilized zirconia (YSZ) have been synthesized using the plasma spray process for solid oxide fuel cell (SOFC) applications. These particles were prepared from zirconium oxynitrate hydrate and yttrium nitrate hexahydrate as precursors. The zirconia particles were spherical and about 100-200 nm in size(*58*).

4.4. Role of slurry in Chemical Mechanical Polishing

As discussed in previous sections, the slurry is one of the important process variables in the process of chemical mechanical planarization (CMP). Slurry parameters such as solution chemistry, abrasive size and concentration, pH, temperature, flow rate, presence of oxidizers, surfactants and corrosion inhibitors etc., influence the planarization process to a great extent. The slurry formulation is done in order to achieve high removal rates, low coefficient of friction, and low defectivity, among other targets(*12*). Though the slurry is responsible in bringing about the chemical aspects of polishing, the interaction of the slurry with the wafer is a very complex mechanism. During polishing, frictional forces come into play when the slurry flows between the polishing pad and the

wafer. These result in mechanical removal of material producing defects. If the frictional forces are lowered, the removal rate also decreases. So, the process has to be optimized to achieve high planarity with minimum defects. Slurry choice has a great effect on the manufacturing, yield and reliability of the process.. Commercial CMP slurries are now being customized for specific process applications.

4.4.1. Slurry composition

Slurries consist of dispersed abrasive particles along with certain chemical reagents to bring about the selectivity for metal CMP. The solution acts as a lubricant, controlling the temperature and transports chemical reagent for the abrasives and the chemical reagents to the polishing site. These chemical reagents include oxidizers, surfactants, chelating agents, complexing agents, buffer solutions etc. Slurries for metal CMP contain more additives than oxide CMP. The solution also provides electrostatic and steric balance for suspending the abrasives. For electrostatic stabilization, zeta potential is important for determining the stability of the slurry while for steric stabilization, the choice of the molecule is more important. This is because, electrostatic stabilization results from the repulsion between the like charges while steric stabilization is a result of physical interaction of high-molecular weight species.

4.4.2. Abrasives in slurry

The role of the abrasive is to provide the mechanical aspect of CMP (*73*). These particles act by abrading the dull and uneven surface. The first generation metal CMP used alumina abrasives and the first generation oxide CMP consisted of fumed silica

particles. The abrasives are required to meet certain criteria of correct chemical properties, hardness and surface charge.

1. Alumina as a slurry abrasive: Alumina has been used in metal CMP for producing higher removal rates. Studies have shown that both, phase and hardness of the alumina particles affects the polishing. Due to the high hardness of the alumina particles, additional measures need to be taken to reduce the surface defects on wafers.
2. Silica as a slurry abrasive: Since, alumina particles showed high defectivity, silica abrasives have been the next method of choice. The silica abrasives used for the CMP process are fumed and colloidal particles. Both forms are amorphous in nature. Polishing with colloidal silica has shown lower defectivity while slurries containing fumed silica have shown higher removal rates.
3. Ceria as a slurry abrasive: Ceria slurries are gaining importance in the field of oxide CMP. Owing to high removal rates, ceria slurries are extensively being used for shallow trench isolation (STI) (*73*).

Apart from the type of abrasive being used in the slurry, the particle properties such as size and hardness also play an important role. As the particle size and hardness of the abrasive particles in the slurry increases, the removal rate increases. The same effect is seen with the increase in the number of abrasive particles in the slurry. Bigger abrasive particles produce deeper surface defects such as micro-scratches. Research has shown that removal rates tend to decrease after a particular size threshold of the abrasive particles (*35*) .

4.5. Research focus: synthesis, characterization and applications

As already discussed in the previous sections, abrasives play an important role in the CMP slurry. The objective of this research is to investigate the effect of zirconia nanoparticles as abrasives in the CMP slurry. Zirconia nanoparticles used in the slurry preparation were successfully synthesized through the Plasma route.

Zirconia nanoparticles were synthesized using the plasma route. The set up can be divided in to three segments. The first segment is the precursor delivery. Zirconium butoxide was used as the precursor and was fed to the plasma torch in the vapor form. The second segment is the plasma chamber where the precursor gets decomposed. The third segment is the powder collection chamber. The plasma torch is characterized by plasma tube surrounded by high velocity cooling-water, to protect against the heat. The induction coil in the torch is connected to the RF power supply which generates the discharge.

Different sets of gases are introduced in the chamber. The sheath gas reduces the heat flux and is directed near the ceramic tube. The central gas accounts for plasma stability and is introduced tangentially in the chamber. The precursor, in the vapor form, is introduced in the chamber axially by means of stainless steel tubing. The powder evaporated in the induction plasma torch at high temperatures rapidly solidifies on quenching. The powder is then collected from the collection chamber. The properties of the nanopowders depend on the various parameters such as concentration of the solution and feed rate, plasma properties like composition and power, gas compositions and quenching rates (*58*)

The synthesized nanoparticles were used to make the abrasive slurry. The slurry was made by dispersing the zirconia abrasive particles 3% by weight in de-ionized water. 0.2 mmol of tetramethyl ammonium hydroxide (TMAH) was added. The slurry was then used to polish 2 inch oxide wafers against the 6 inch polishing pad on the CETR bench top tester. The in-situ coefficient of friction was monitored during the process.

Zirconia nanoparticles synthesized by the plasma route were characterized using various analytical techniques. XRD was done to analyze the crystallographic structure and chemical composition. TEM was done to understand the shape, structure and size of these nanoparticles. After the polishing experiments, optical microscopy and AFM was used to analyze the polished oxide wafers for defects.

4.6. Results and discussion

Characterization of zirconia nanoparticles was done to understand the particle structure. Figure 4.1 shows the TEM images of the synthesized nanoparticles at various magnifications. The zirconia nanoparticles were seen to occur in clusters. These particles show a near spherical shape with the particle size ranging from 20 nm to 70 nm. Figure 4.2 shows X-ray diffraction analysis of the zirconia particles. A major peak is seen at $2\theta = 30^{o}$ which is a characteristic of the tetragonal zirconia. Tetragonal phase (101 orientation) was seen to be primarily present followed by traces of the monoclinic phase (-111 and 111 orientation). The widened peaks suggest a crystalline structure.

The synthesized zirconia nanoparticles were used to make the abrasive slurry to polish the oxide wafers. The slurry was made by dispersing the zirconia nanoparticles in DI water. TMAH was added as a surfactant to the slurry. Surfactants are organic

compounds that are added to improve the stability of the slurry (*74*). The experiments were carried out on the CETR bench top tester. The working details of the tester are described in the earlier section. The experimental details of the polishing experiments are listed in Table 4.1. The zirconia particles showed a high settling rate and were seen to deposit in the pipe and so the slurry flow rate was kept high. The in-situ coefficient of friction was monitored and was found to be 0.6 which is unexpectedly high.

Optical microscopy was used to analyze the polished wafer for surface defects that are caused primarily because of the continuous contact of the abrasives with the wafer. The optical images (Figure 4.3) show many scratches and pits on the wafer. The scratches were of varied sizes and were isolated as well as in clusters. The wafer surface appeared rough instead of smooth and planarized. This could be due to the high slurry flow rate that was maintained in order to prevent the particles from settling even before reaching the wafer surface.

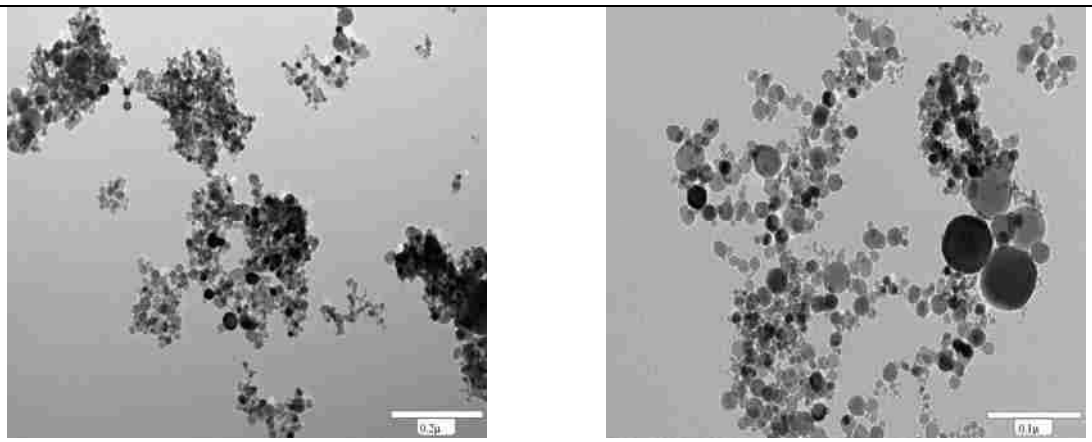

(a) (b)

Figure 4.1: TEM images of zirconia nanoparticles at different magnifications

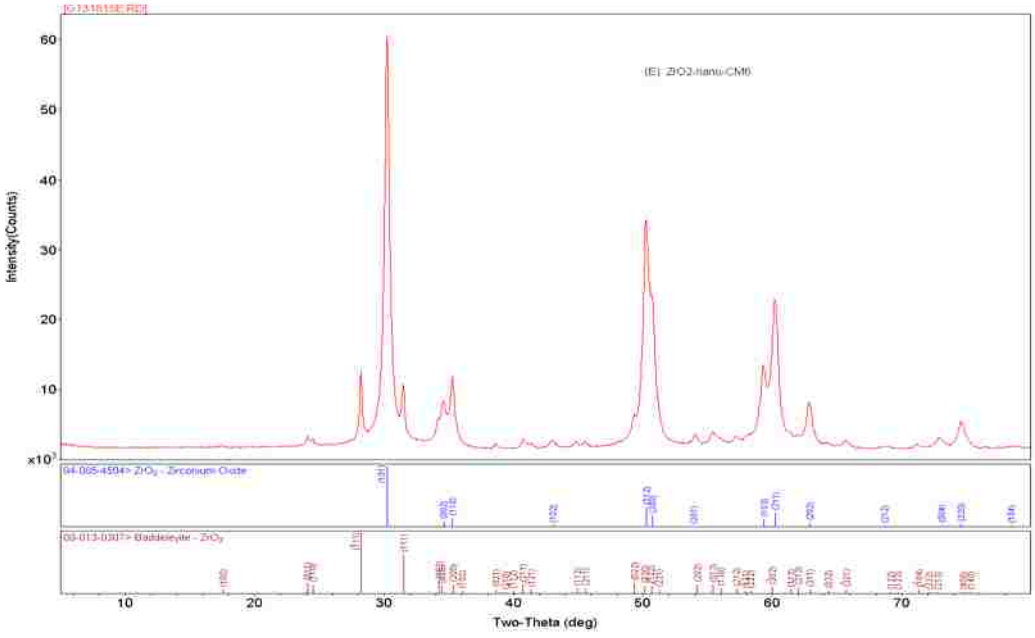

Figure 4.2: XRD analysis of zirconia nanoparticles

(a)

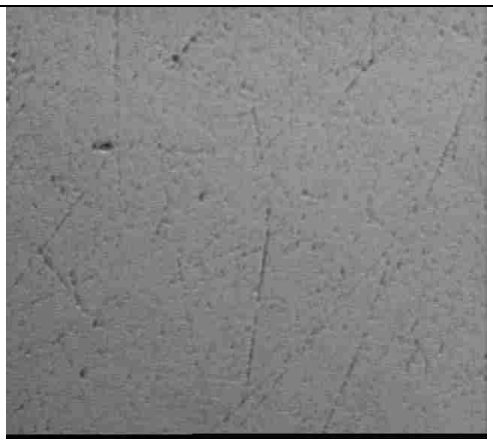

(b)

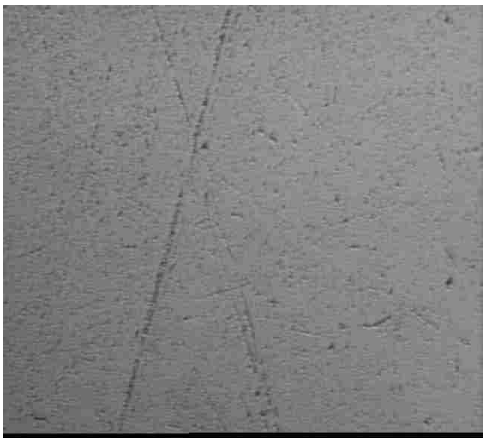

(c)

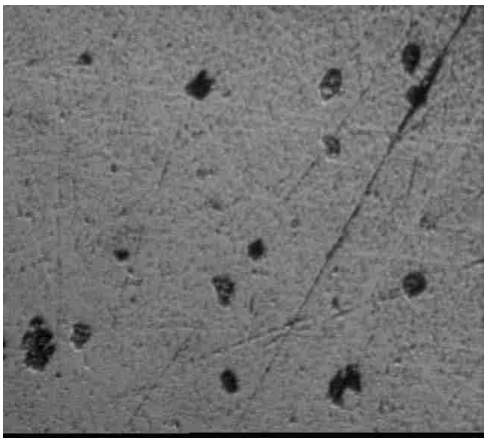

(d)

Figure 4.3: Optical images showing different regions of the wafer polished with zirconia slurry

Table 4.1: Experimental details

Parameter	Value
Slurry	3 wt% zirconia dispersed in DI water
Slurry flow rate	150 ml/min
Pad	Rodel IC 1000, SUBA IV
Down Pressure	3 PSI
Platen speed	150 rpm

Chapter 5

Conclusion

Chemical Mechanical Polishing is a process for achieving local and global planarization. The consumables involved in the process are a subject of extensive studies to understand their effect on the output parameters such as material removal rate, polishing uniformities and surface defects.

The polishing pad made of polyurethane material is one of the major consumable. The pad surface degrades over time with polishing and needs to be regenerated to restore its properties in order to sustain good removal rates and polishing uniformity. This regeneration is done by using abrasive disks, to carry out a process known as conditioning. The abrasives abrade the pad surface to unclog the pores. The size of the abrasives on these conditioning disks plays a major role in determining the conditioning efficiency. In order to understand the impact of these abrasives on the pad, abrasives of different sizes were used in this thesis to carry out the conditioning and the results were quantified in terms of pad roughness, coefficient of friction, and pad wear.

A systematic study of conditioner abrasives ranging in size from 0.25 μm to 100 μm was performed. The results showed that the conditioning with bigger abrasives gave higher pad roughness. For example, the pad roughness upon conditioning with abrasives of size 100 μm was nearly twice that obtained using 0.25 μm abrasives. The roughness

value was also found to increase with increase in conditioning time from 5 minutes to 20 minutes. However, the bigger 100 μm abrasives, when used for a longer conditioning time, start to rupture the pad. Also, for these bigger abrasives, the longer conditioning times led to higher pad wear, which has important consequences such as reduced pad life. The 68 μm and 100 μm conditioner abrasives also showed a high value of COF (0.5-0.7) during conditioning, which was nearly twice the value found for the smaller abrasives. Though the smaller abrasives showed a steady increase in the COF values with an increase in conditioning time, the change in COF value for bigger abrasive was nearly negligible. These results of the systematic study in this thesis indicate that smaller abrasives need longer conditioning times to achieve same degree of pad abrasion as the bigger conditioning abrasives.

The bigger abrasives (8 μm, 68 μm, 100 μm) were used to carry out the ex-situ conditioning for polishing the copper wafers and the effect of pad conditioning was observed on the polished wafers. More surface defects were found on the wafers that were polished using the pads conditioned with the 100 μm abrasive while the pad conditioned with the smaller 8 μm abrasive gave comparatively less scratches. It was also noted that for the same polishing time, the end-point for polishing was achieved when using the pad conditioned with the 100 μm conditioning abrasive and not for the pad conditioned with the 8 μm conditioning abrasive. This result indicates that differences in conditioning can lead to steady state at different times during polishing. Thus, optimization has to be achieved between conditioning times and size of the conditioning abrasive as it impacts the pad life, the pad properties and finally the surface defects during polishing.

For future work, it will be interesting to look at the time needed for the smaller abrasives (0.25 μm and 2 μm) to show the same COF and pad roughness as shown by the bigger abrasives. Since smaller abrasives can reach the pores of the polishing pad and can prove more effective in unclogging them, it will be interesting to see if an increase in the density for the smaller abrasives gives better polishing results. Higher pad roughness has been reported to give high removal rates. So, another focus for future evaluation of abrasive conditioning would be to look at the material removal rate, which is an important CMP output parameter. High removal rates indicate good pad properties and a better CMP performance.

Another major contribution of this thesis has been in the development of a simple method to measure pad-wafer contact area. Since pad morphology was found to be affected by conditioning and the degree of change in the pad morphology depended on the conditioner abrasive size, the effect of pad morphology on contact area was investigated using a simple optical method. Optical microscopy was used to analyze the pad-wafer contact area. The contact area was seen to increase with an increase in pressure. The preliminary work presented here has demonstrated that optical microscopy can be a simple yet effective technique to measure the contact area and allow future work on measurement of contact area as a function of the pad conditioning process.

Finally, to understand the effect of abrasives in the slurries for CMP, zirconia nanoparticles (as abrasives) were synthesized through the plasma route. The wafer polished with these nanoparticle slurries exhibited many surface defects such as pits and scratches. As many input variables work simultaneously in producing these results, these surface defects could be a result of high slurry flow rate, the relative platen speed, or the

set down pressure. Further experiments need to be done to understand the effect of the zirconia based slurry and the interplay with the other input variables. Here, the first step would be to focus on the slurry chemistry as it plays a very important role in polishing the wafer. With a high settling rate of zirconia particles in the slurry, appropriate chemical additives need to be added to prevent the agglomeration and settling of the particles. Optimization of the input variables such as platen speeds and slurry flow rate will also improve the wafer polishing. An evaluation of the effectiveness of the zirconia slurry can then be performed by measuring the material removal rate after polishing.

References

1. J. M. Steigerwald, S. P. Murarka, R. J. Gutmann, *Chemical Mechanical Planarization of Microelectronic Materials*. (Wiley-Interscience, 1997).

2. J. Olsen, F. Moghadam, *Handbook of Multilevel Metallization for Integrated Circuits: Materials, Technology, and Applications*, (1993).

3. S. Wolf, R. N. Tauber, *Pattern Registration*, 473 (1986).

4. K. Kobayashi, *Journal of Physics and Chemistry of Solids* **59**, 1671 (1998).

5. K. Kobayashi, *Materials Science & Engineering B* **98**, 181 (2003).

6. J. Levert, S. Mukherjee, D. DeBear, in *Electrochemical Society Conference*. (Hawaii, 1999).

7. J. H. Zhao *et al.*, *Applied Physics Letters* **74**, 944 (1999).

8. D. Evans, *Materials Research Society Bulletin* **27**, 779 (2002).

9. J. W. Carr *et al.* (EP Patent 0,401,147, 1990).

10. F. W. Preston, *Journal of the Society of Glass Technology* **11**, 214 (1927).

11. C. W. Liu, B. T. Dai, C. F. Yeh, *Journal of the Electrochemical Society* **142**, 3098 (1995).

12. Z. Li, K. Ina, P. Lefevre, I. Koshiyama, A. Philipossian, *Journal of the Electrochemical Society* **152**, G299 (2005).

13. Z. Li, L. Borucki, I. Koshiyama, A. Philipossian, *Journal of the Electrochemical Society* **151**, G482 (2004).

14. K. H. Park, H. J. Kim, O. M. Chang, H. D. Jeong, *Journal of Materials Processing Technology* **187**, 73 (2007).

15. L. M. Cook, in *Semiconductors and Semimetals*. **63** (2000).

16. M. R. Oliver, *Chemical-Mechanical Planarization of Semiconductor Materials*. (Springer, 2004).

17. L. M. Cook, J. V. H. Roberts, C. W. Jenkins, R. R. Pillai. (US Patent 5,489,233, 1996).

18. R. Bajaj, M. Desai, R. Jairath, M. Stell, R. Tolles, *Materials Research Society Proceedings* **337**, 637 (1994).

19. R. Kolenkow, R. Nagahara, *Solid State Technology* **35**, 112 (1992).

20. I. Ali, S. R. Roy, G. Shinn, *Solid State Technology* **37**, 63 (1994).

21. R. Jairath, M. Desai, M. Stell, R. Tolles, D. Scherber-Brewer, *Materials Research Society Symposium* **337**, 121 (1994).

22. R. Dejule, *Semiconductor international* **20**, 54 (1997).

23. J. Grillaert *et al.*, *Materials Research Society Proceedings*, 45 (1999).

24. M. R. Oliver, R. E. Schmidt, M. Robinson, *Chemical Mechanical Planarization IV: Proceedings of the International Symposium*, (2001).

25. C. Y. Chen, C. C. Yu, S. H. Shen, M. Ho, *Journal of the Electrochemical Society* **147**, 3922 (2000).

26. J. Z. Zhang *et al.*, in *CMP-MIC* (1997), pp. 315-321.

27. B. J. Hooper, G. Byrne, S. Galligan, *Journal of Materials Processing Technology* **123**, 107 (2002).

28. T. S. Bullard, R. J. Lebel, R. Nadeau, P. H. Smith Jr. (US Patent 6,022,266, 2000).

29. N. H. Kim, Y. J. Seo, W. S. Lee, *Microelectronic Engineering* **83**, 362 (2006).

30. T. Sun, L. Borucki, Y. Zhuang, A. Philipossian, *Materials Research Society Symposium Proceedings* **991**, 45 (2007).

31. K. H. Park, H. J. Kim, O. M. Chang, H. D. Jeong, *Journal of Materials Processing Tech.* **187**, 73 (2007).

32. H. Lu, Y. Obeng, K. A. Richardson, *Materials Characterization* **49**, 177 (2002).

33. T. Murayama, *Dynamic Mechanical Analysis of Polymeric Material*. (Elsevier Scientific Pub. Co., 1978).

34. Y. R. Jeng, P. Y. Huang, W. C. Pan, *Journal of The Electrochemical Society* **150**, G630 (2003).

35. R. K. Singh, R. Bajaj, *Materials Research Society Bulletin*, 743 (2002).

36. J. A. Greenwood, J. B. P. Williamson, *Proceedings of the Royal Society of London. Series A* **295**, 300 (1966).

37. G. B. Basim, I. U. Vakarelski, B. M. Moudgil, *Journal of Colloid and Interface Science* **263**, 506 (2003).

38. C. L. Elmufdi, G. P. Muldowney, *Materials Research Society Symposium Proceedings* **991**, 15 (2007).

39. C. Gray *et al.*, *Materials Research Society Symposium Proceedings* **991**, 27 (2007).

40. C. Gray *et al.*, *Materials Research Society Symposium Proceedings* **867**, 247 (2005).

41. R. Mueller, R. Jossen, S. E. Pratsinis, M. Watson, M. K. Akhtar, *Journal of the American Ceramic Society* **87**, 197 (2004).

42. L. A. T. Hartmann W., Peuckert D. and Kleinschmit, *Materials Science and Engineering, A.* **109**, 243 (1989).

43. O. Flame, *Ultrafine Particles*, (1963).

44. J. Karthikeyan *et al.*, *Nanostructured Materials* **8**, 61 (1997).

45. F. L. Yuan, C. H. Chen, E. M. Kelder, J. Schoonman, *Solid State Ionics* **109**, 119 (1998).

46. K. A. a. M. T.F., *Aerosol Sci. Technol.* **34**, 227 (2001).

47. S. D. Ramamurthi, Z. Xu, D. A. Payne, *Journal of the American Ceramic Society* **73**, 2760 (1990).

48. C. Y. Tai, M. H. Lee, Y. C. Wu, *Chemical Engineering Science* **56**, 2389 (2001).

49. M. Z. C. Hu, M. T. Harris, C. H. Byers, *Journal of Colloid And Interface Science* **198**, 87 (1998).

50. V. V. Srdic, M. Winterer, A. Moller, G. Miehe, H. Hahn, *Journal of the American Ceramic Society* **84**, 2771 (2001).

51. J. Livage, F. Beteille, C. Roux, M. Chatry, P. Davidson, *Acta Materialia* **46**, 743 (1998).

52. T. Mimani, K. C. Patil, *Materials Physics and Mechanics(Russia)* **4**, 134 (2001).

53. M. Yoshimura, S. Somiya, *Materials Chemistry & Physics* **61**, 1 (1999).

54. J. D. Lin, J. G. Duh, *Journal of the American Ceramic Society* **81**, 853 (1998).

55. S. Somiya, T. Akiba, *Journal of the European Ceramic Society* **19**, 81 (1999).

56. A. Cabanas, J. A. Darr, M. Poliakoff, E. Lester, *Chemical Communications* **2000**, 901 (2000).

57. G. Skandan, *Nanostructured Materials* **5**, 111 (1995).

58. Z. Wang *et al.*, *Journal of Power Sources* **170**, 145 (2007).

59. L. Tong, R. G. Reddy, *Journal of the Minerals, Metals and Materials Society* **58**, 62 (2006).

60. G. Vissokov, I. Grancharov, T. Tsvetanov, *Plasma Science and Technology* **5**, 2039 (2003).

61. P. Madhu Kumar *et al.*, *Materials Chemistry and Physics* **36**, 354 (1994).

62. S. M. Oh, D. W. Park, *Thin Solid Films* **386**, 233 (2001).

63. Y. L. a. T. Ishigaki, *Thin Solid Films* **407**, 79 (2002).

64. G. a. P. P. Vissokov, *Ultradispersed powders Plasma-chemical Preparation and Properties*, 395 (1998).

65. S. J. Gubzica J, Mahai I, et al, *Journal of Materials Science* **35**, 3711 (2000).

66. K. P. a. P. E. Chang Y, *Plasma Chemistry and Plasma Processes* **9**, 73 (1989).

67. H. B. Liang S, Zheng Z, et al, *Trans. Nanoferrous Metals Society, China* **3**, 103 (1996).

68. C. Y. Young R M, Lecerf B, et al, *8th International Symposium on Plasma Chemistry, Tokyo* **4**, 2040 (1987).

69. K. N. a. S. K. Futaki S, *8th International Symposium on Plasma Chemistry, Tokyo*, 2040 (1987).

70. G. F. Guo J Y, Boulos M I, *Plasma Chemistry and Plasma Processing* **17**, 219 (1997).

71. G. F. Guo J Y, Boulos M I, et al, *Journal of Materials Science* **32**, 5257 (1997).

72. D. Vollath, D. V. Szabó, *Journal of Aerosol Science* **28**, 685 (1997).

73. L. M. Cook, *Journal of Non-Crystalline Solids* **120**, 152 (1990).

74. Y. Hong, U. B. Patri, S. Ramakrishnan, S. V. Babu, *Chemical-Mechanical Planarization--Integration, Technology and Reliability* **867**, 41 (2005).